2024

Using remote sensing to track complex sinuous ripple migration on a barchan dune in Herschel Crater, Mars

Visick, Elizabeth

UNIVERSITY OF PLYMOUTH

Using remote sensing to track complex sinuous ripple migration on a barchan dune in Herschel Crater, Mars

by

Elizabeth Sarah Visick

A thesis submitted to the University of Plymouth

in partial fulfilment for the degree of

RESEARCH MASTERS

School of Geography, Earth and Environmental Sciences

March 2023

Acknowledgments

I would like to acknowledge and give my thanks to my supervisors (Matt Telfer and Martin Stokes) who made this work possible.

I would also like to recognise the patience, support and motivational speeches my family, partner and friends have had to give me over the past year. This has been a difficult but highly rewarding journey for myself and everyone around me.

Author's Declaration

At no time during the registration for the degree of *Research Masters* has the author been registered for any other University award without prior agreement of the Doctoral College Quality Sub-Committee.

This thesis has been proofread by a third party; no factual changes or additions or amendments to the argument were made as a result of this process. A copy of the thesis prior to proofreading will be made available to the examiners upon request.

Work submitted for this research degree at the University of Plymouth has not formed part of any other degree either at the University of Plymouth or at another establishment.

A programme of advanced study was undertaken, which included the following taught modules:

GEOL5001 Geoscience Frontiers: Research and Communication

GEOL5003 Advanced Analytical Skills

GSRGEOL1 Research Geological Sciences

Word count of main body of thesis: 11,463

Signed: 

Date 22nd of February 2023

Abstract

Using remote sensing to track complex sinuous ripple migration on a barchan dune in Herschel Crater, Mars

by

Elizabeth Sarah Visick

This thesis presents evidence of dune and ripple migration in Central Herschel Crater on Mars. High resolution satellite imagery (25 cm/pixel) was georeferenced and analysed using ArcGIS Pro. It is calculated that the average dune migration rate can reach a distance of 4.2 m per year and an average ripple migration rate of 0.38 m per year. The dune's morphology has been influenced by the prevailing winds from the north, creating a barchan dune with an elongated eastern horn. However, the dunes undulating stoss slope and the complex superimposed ripples is likely caused by a complex wind regime. The dune itself is the most northern located dune in central Herschel Crater. A ridge is located halfway between the dune and the northern crater rim, suggesting that the topography of the crater may be inducing a turbulent wind pattern. This is also evidenced in the migration directions of the superimposed ripples which do not correlate to that of the overall southernly dune migration. To test the significance and reliability of the data, the sensitivity of the analyses parameters to calculate migration distances in ArcGIS Pro was explored using the programming language R. These analyses showed that the search parameter setting did have a significant impact on the migration distances calculated ($p < 0.0001$). This thesis has applied and evaluated a new method for quantifying ripple migration on Mars. The work presented here demonstrates one method that has the potential to help fully utilise existing aerial imagery on Mars.

Contents

List of Acronyms

DTM	Digital Terrain Model
COSI-corr	Co-registration of Optically Sensed Images and Correlation
GCM	Global Circulation Model
GIS	Geographic Information Systems
HiRISE	High Resolution Imaging Science Experiment
IBL	Internal Boundary Layer
MRO	Mars Reconnaissance Orbiter
PBL	Planetary Boundary Layer

List of Figures

List of Tables

1. Introduction

Mars, originally thought to be geologically inactive due to its thin atmosphere, low gravity and from afar featureless surface has in recent history proved the opposite (Heap *et al.*, 2017). The first images of the planet's surface arrived in 1965 from Mariner 4 mission (Daines, 2015). This mission contributed to the research for future potential landing sites and areas of particular interest (NASA Solar System Exploration, 2019). Yet it was not until the Mariner 9's successful mission to Mars that proved Mar's geologically active state after capturing images of a large dust storm (NASA Solar System Exploration, 2019). The mission managed to capture 85% of the planet's surface (NASA Solar System Exploration, 2019), feeding back images of geological features that overtime showed to be moving, i.e., dunes and ripples (Silvestro *et al.,* 2010a; Silvestro *et al.,* 2010b; Silvestro *et al.,* 2010c). The evolving and actively changing geomorphology of dunes and ripples through weathering mechanisms, transport processes, and the development of new features on this planet can develop our understanding of the ancient and modern climate and wind cycle of Mars. As well as creating new technological advances for Martian missions, this is advantageous to Earth's exploratory industries such as mining and to the general scientific community (Nummi, 2016 and European Space Agency, 2003).

Martian wind regimes can be mapped out by using our understanding of the mechanics behind the formation of dunes and ripples on Earth (Favaro et al 2021). However, Martian dunes and ripples bring a new level of complexity to the forming mechanisms of these geomorphological features (Lapotre *et al.,* 2016). Intensive studies on the primary characteristics of airflow over dunes have been carried on Earth using field measurements, numerical simulations and laboratory experiments however very little is known about

Martian airflow as it has been limited to specific dune a ripple morphology (Hood *et al.,* 2012). Ongoing research continuously brings new evidence of how these features on Mars are defying the rules of what we thought should make up these mechanics. Further complications of distinguishing the factors behind the processes of dune and ripple formation is a highly debated subject to this day (Day and Zimbelman, 2021; Lapôtre, Ewing and Lamb, 2021; Sullivan et al., 2020).

Researching the formation of present-day Martian topographical features to understand how they have been influenced by geological weathering and transportation agents today using remote sensing techniques and COSI-Corr can generate an accurate model of how dunes and ripples on Mars are formed and accurately measure their migration (Zheng *et al.,* 2022; Favaro *et al.,* 2021; Banham *et al.,* 2021; Hood *et al.,* 2021; Sostre-Cortes and Diniega, 2021; Silvestro et al., 2020). Furthermore, this could give an insight into the ancient wind cycle and Martian climate (Hood *et al.,* 2021; Hayward, *et al.,* 2014; Fenton, 2003). This potential advance in scientific knowledge could bring to light new intelligence on the Martian atmosphere, wind cycles and geological knowledge that may serve well in new Martian exploration missions.

The development of the High Resolution Imaging Science Experiment (HiRISE) aboard the Mars Reconnaissance Orbiter (MRO) demonstrates that geomorphological features on Mars' surface can be actively tracked evidence their continuous activity to this day. Research of dune and ripple migration has been strongly focused on areas of large dune fields as there is the opportunity for wide data collection and analysis, such as the Bagnold dune fields and east and western Herschel Crater. While areas where there are isolated dunes are often not researched. Central Herschel Crater presents areas of isolated dunes or very small groups of dunes of which little, to no research has been carried out on them.

An algorithm for crestline detection for ripples on Mars using HiRISE imagery inserted into ArcGIS Pro 2.9.5 (Geographic Information Systems) is a quick and effective way to confirm spatial migration of ripples (Telfer *et al.*, 2015).

1.1 Aims and objectives

This research project aims to detect and quantify sinuous longitudinal large ripples on barchanoid bedforms, Herschel Crater, Mars. Sinuous longitudinal ripples are formed parallel to the wind direction. These ripples have a complex morphology which is rarely seen on Mars to date and are not present to the same extent on Earth. Therefore, this research project will examine how known aeolian processes on Earth could be applied to Mars.

To achieve this aim, this research project comprises the following specific objectives:

1. Conduct a literature review on terrestrial aeolian theory and how this theory has informed ripple detection methods applied to Martian satellite imagery.
2. Acquisition and georeferencing of high spatial resolution (25 cm) Mars Digital Terrain Model (DTM) for Herschel Crater, Mars between 2010 and 2017.
3. Apply a modified algorithm for crestline detection using ArcGIS Pro 2.9.5 and subsequently quantity migration rates.
4. Undertake a statistical method sensitivity analysis of ripple migration rates using the programme language R.
5. Interpretation of migration rates linked wind direction and sediment availability and how this could influence complex ripple patterns.

2. Literature Review

2.1 Mars's Geological History

The Martian climate has been sculpted by many geological agents over the past 4 billion years (Carr and Head, 2010; Hartmann and Werner, 2010; Neukum *et al.,* 2010) (Figure 2.1). It was heavily cratered during the Late Heavy Bombardment (Cabrol and Grin, 2010) an increase in meteor impacts on the planet's surface throughout a certain period of time (Bottke and Norman, 2017). Episodes of large flood waters towards the end of the Noachian period (4.1 Ga – 3.7 Ga) and throughout the Hesperian (3.7 Ga – 3.1 Ga) (Salvatore and Levy, 2021; Carr and Head, 2010; Chapman *et al.,* 2010) are evidenced by a network of valleys and sulphate rich deposits (Carr and Head, 2010). Throughout the Noachian and Hesperian volcanic activity dominated the planet (Salvatore and Levy, 2021; Carr and Head, 2010; Neukum *et al.,* 2010). During the Amazonian period (3.1 Ga – present), evidence of water and volcanism as the main geological agent acting on Mars significantly decreased and the period is characterised by weathering and erosion, from the destabilisation of valleys and other steep topographical features and the formation and movement of ice (Carr and Head, 2010; Chapman *et al.,* 2010).

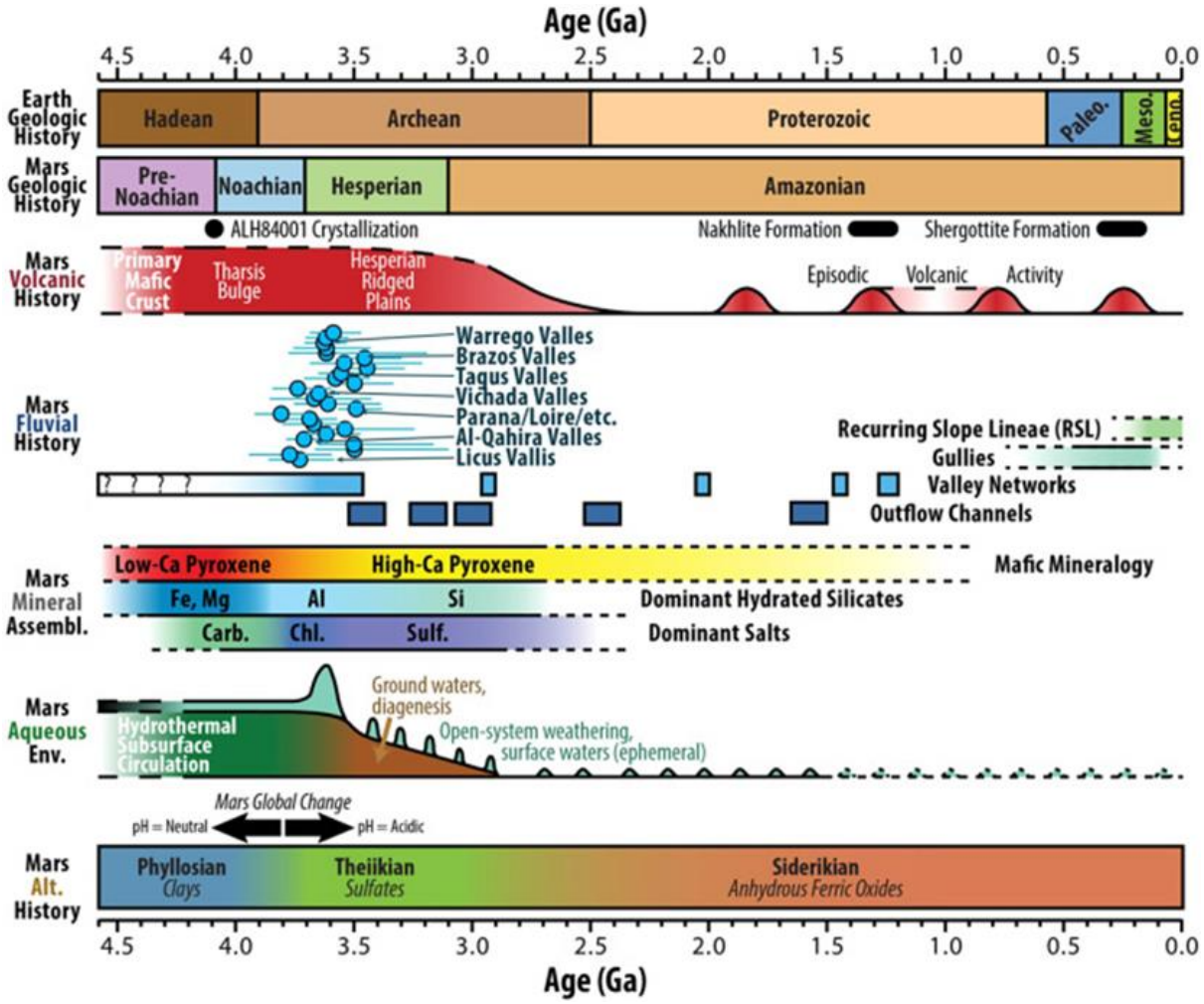

Figure 2.1 The geological timeline of Mars (Salvatore and Levy, 2021).

Furthermore, the surface topography is split into two distinctive hemispheres 'Martian dichotomy', the northern lowlands and southern highlands (Cheng et al., 2021; Smrekar, 2004) (Figure 2.2). The northern lowlands are an area of which has been resurfaced over a heavily cratered landscape, evidenced by a gravity field survey. It is the largest even topographical feature in the known solar system. The southern highlands hold the oldest geology indicating a more stabilized crust earlier on in Martian history (Smrekar, 2004; Zuber, 2000).

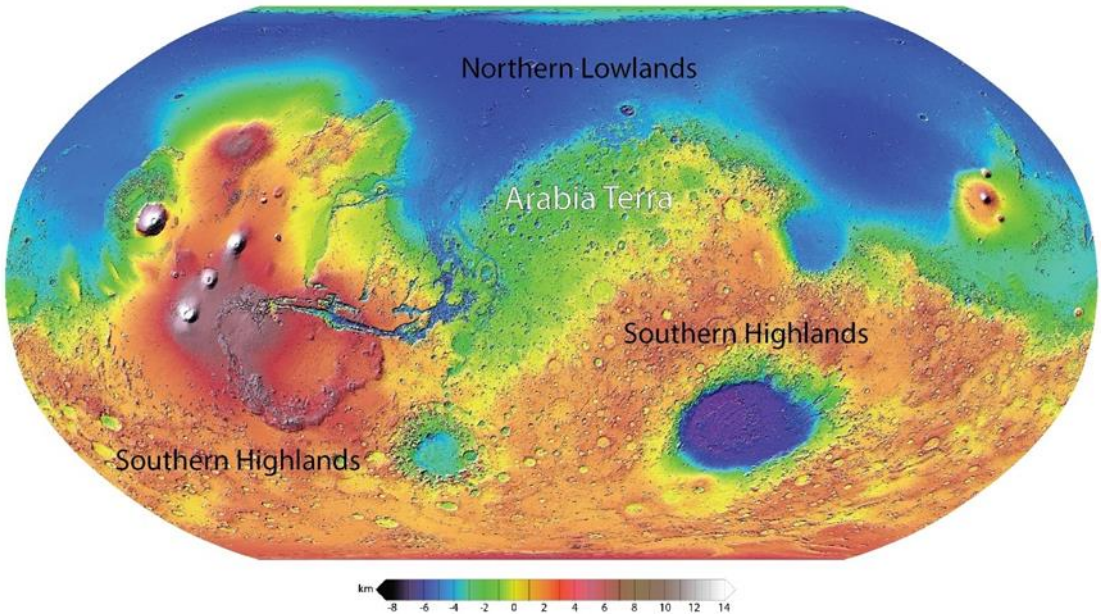

Figure 2.2 A topographical map for Mars. Image sourced from (The Planetary Society, 2022).

2.2 Sediment transport on Mars

Today, aeolian processes are the dominant acting agents on the Martian surface, this is evidenced by global and localised dust storms, dust devils and geomorphological features present i.e., dunes and ripples (Fenton, 2003; Renno, Wong and Atreya, 2003). Global dust storms that circulate the whole planet are usually initiated in the mid-to-low latitudes of the planet propagating eastward while continual development occurs in the southern latitudes (Cantor, 2007). A global dust storm occurred in June 2006 evidencing several areas of dust entrainment reaching ~60 km altitude in some areas (Cantor, 2007). The most recent global dust storm event was in 2018 (Kass et al., 2020; Guzewich et al., 2019; Smith, 2019). However, smaller scale storms, also known as regional storms, happen more regularly with the most recent (at the time of writing) being detected by NASA's InSight lander in January 2022 (mars.nasa.gov, 2022). Further evidence of sediment transport through wind is from dust

devils in photos like the one captured by the Curiosity rover August 2020 (JPL NASA, 2020) (Figure 2.3). Lastly, one of the other major features evidencing current aeolian activity on Mars are the migrating dunes and ripples (Bridges et al., 2017; Silvestro et al., 2011; Silvestro et al., 2010). The dunes and ripples are a testimony of current wind direction on a regional and local scale and the dune morphology evidences the variation of wind directions i.e., unidirectional and bidirectional winds (Lapôtre, etal., 2021; Vaucher and Dashtgard, 2021; Sullivan et al., 2020).

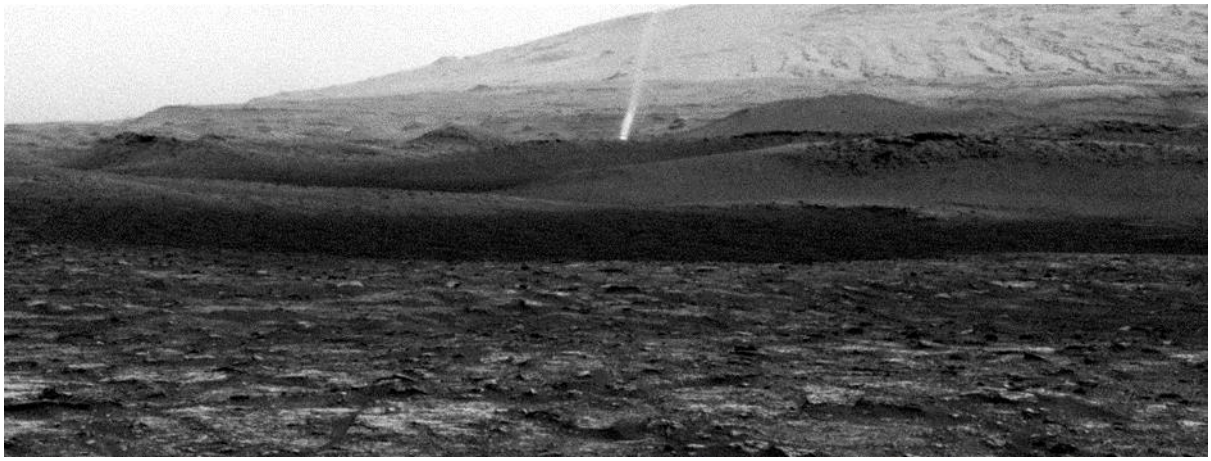

Figure 2.3 Photographic evidence of dust devil taken by the Mars Curiosity Rover (JPL NASA, 2020).

Dunes and ripples on Mars are on a much larger scale than those found on Earth (Day and Zimbelman, 2021). Differentiating the dunes and in particular the ripples on Mars have been much debated. However, Day and Zimbelman (2021) categorized the majority of the aeolian features seen in satellite imagery (Table 2.1) however smaller scale features are not identifiable from orbital imagery and the mechanics behind bedform formation is still being widely researched. But from the study of aeolian influenced landscapes on Earth, such as the dune fields (also known as sand seas/ergs) of the Sahara, Australia, southern Africa and the

Central Asia enclosed basins (Lancaster and Mountney, 2021 and McKee 1979), we can determine the basic requirements that from these geomorphological features. For sediment to be available to form growing dunes and ripples there must be an erodible bed being mobilized by a fluid flow (Charru et al., 2013 and Bagnold 1941).

2.3 Ripples

Ripples are a geomorphological feature, which even on Earth the forming mechanisms are still evolving through ongoing research (Hughes *et al* 2010). However, research does dominantly show that ripples can evidence wind regime, sediment type and sediment availability (Diniega *et al.,* 2021). It is important to note that on Earth the formation of ripples varies dependant on whether it is formed through oscillatory motion via waves (subaqueous) or that is formed by air flow (subaerial).

Large Martian ripples are a highly discussed topic within the geomorphology world. Many researchers have studied large Martian ripples to understand their formation and dynamics (Lapotre et al 2016, Bagnold 1941, Greely and Iverson, Yizhaq, Saban and Katra 2020 Bridges, sharp 1963, Anderson 1987, Day and Zimbelman, 2021). Ripples on Mars have a more complex nature as there is much debate over their characterisation and formation, therefore it has been difficult to classify them when trying to explain the aeolian features observed on Mars (Day and Zimbelman, 2021), while on Earth most ripples have been classified (Figure2.6). Ripples are a small sedimentary bedform and are produced under overall low energy conditions (Dijk *et al*, 2021; Vaucher and Dashtgard, 2021) However, unidirectional ripples form under a relative high energy condition that are oscillatory (Venditti, 2005).

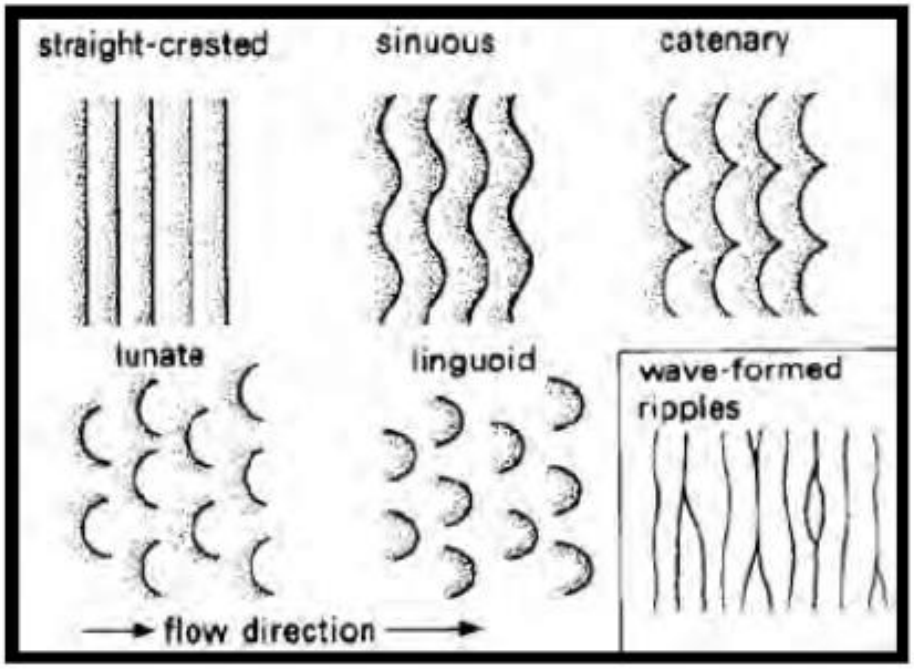

Figure 2.6 Classification of ripples that are found on earth (Hughes *et al.,* 2010).

Initiation of bedforms is still not fully known however research carried out by Venditti (2005) describes that it can come from the build-up of sediment mounds in a channel. Other studies show ripple development is when an unstable flatbed or/with a potential obstacle allows the build-up of fine sands leading to the formation of unimodal ripples (Lammel *et al.,* 2018; Yizhaq *et al*., 2012, cited in Siminovich, 2019; Sullivan *et al.,* 2020). Terrestrial ripple sizes are dependent on 4 fundamental components evidenced by previous research; grain size frequency, wind direction, wind strength and the environment in which they are in (Siminovich *et al.,* 2019). However, megaripples are formed where there are bimodal sands, usually accumulating where there is a larger ratio of coarse to fine sands and these are often found in areas between dunes. (Lammel *et al.,* 2018; Yizhaq *et al*., 2012, cited in Siminovich, 2019; Wang *et al.,*2019; Yizhaq and Katra, 2015; Day and Zimbelman, 2021; Silvestro *et al.,* 2020; Sullivan *et al.,* 2020; Tholen *et al.,* 2022).

Bridges (2013) assumed that using terrestrial analogues, ripples superimposed on dunes must be composed of finer sands than those forming on sand sheets. An example of this effort to understand initiation of development of ripples is through wind tunnel experiments that have been conducted to aid research for both Earth and Mars, however, while most can be directly applied to Earth, Martian conditions is extremely difficult to simulate and is not easy or cost-effective to do (Bridges, 2015. Therefore, using the knowledge we have gained from terrestrial ripples as analogues, adaptation of our understanding of the mechanics behind the initiation and development of ripples can be modified for Mars i.e., gravity (Bagnold, 1941). The mechanics behind ripple formation first started with Bagnold's (1941) theory where the height of the ripple is directly linked to the height of the saltating grains of sand. Bagnold's wind tunnel experiment for the formation of large wind/fluid drag ripples uses 80µm beads in a wind tunnel experiment resulted in a transition of small to large fluid drag ripples when wind velocity exceeded u_* = 0.3 m/s creating wavelengths of λ = 1.5 cm (Figure 2.5 and 2.6). Wind tunnel experiments carried out by Bridges *et al.,* (2015) shows that coarse grains surround a fine-grained core like the Puna megaripples. Clasts are moved by wind gusts and the saltation process reduces the threshold of entrainment, this is first stage of ripple formation (Bridges *et al.,* 2015). They tend to nucleate as material clumps, which protects the finer sediment in the interior, showing intermittent creep is the factor that causes this and has been supported by studies in the Wright Valley, Antarctic, and gravel megaripple formation (Bridges et al 2015). Once the ripple has formed with the finer interior and coarse armouring exterior of particles the feature tends to be stable, only moving due to strong gusts of wind.

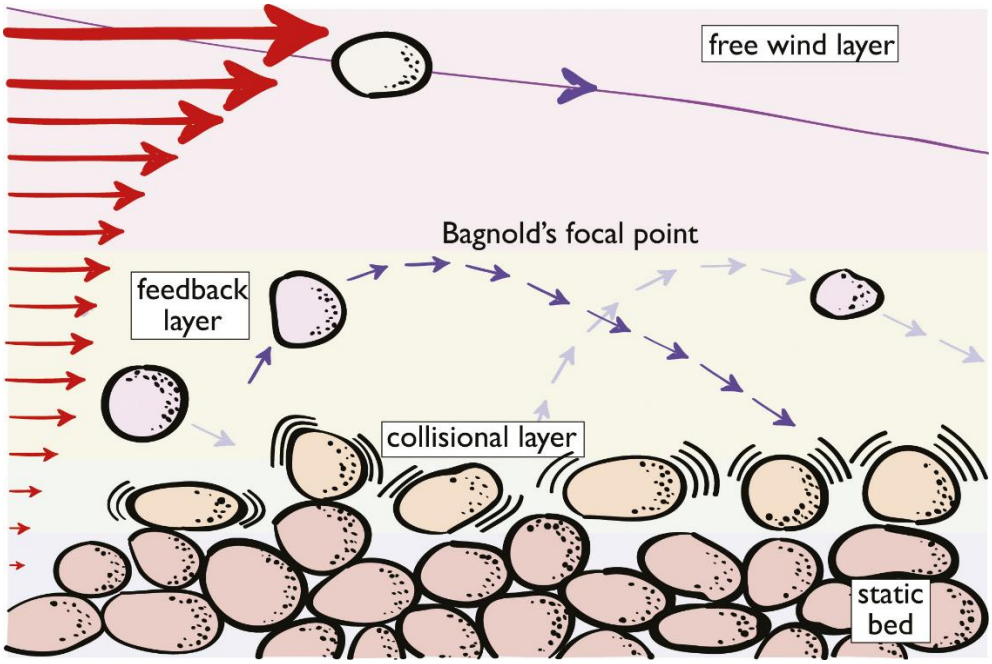

Figure 2.4 Bagnold's theory of sediment transport for ripple formation. Image sourced from (Andreotti et al., 2021).

Development of and challenges against Bagnold's (1941) theory have been carried out through further experiments and research by Sharp (1963). Sharp (1963) understood that the evolution of ripple wavelength is principally reliant upon the development of ripple amplitude and impact angle of the saltating grains on the bed, where the controlling factors are argued based on geometric qualitativeness of grain size and air velocity (Zimbelman, Williams and Johnston, 2012; Anderson 1987). Wilson (1972) and Ellwood, Evans and Wilson (1975) further developed Bagnold's theory by encompassing bimodal or poorly sorted sand, concluding that ripple wavelengths correspond to the mean length of saltating grains (as cited by Anderson, 1987). In 1981 Walker experimented with existing aeolian ripple concepts and using his thorough knowledge of the subject area, directed attention to the fact that the principle of 'ripple wavelength is directly linked to characteristic path length' is far too simple (Anderson, 1987). This leads to Anderson's analytical model in which he used previous works carried out

by ‘Rumpel, 1985; Mitha et al., 1986; Anderson & Hallett, 1986; Ungar & Haff, 1987; Willetts & Rice, 1986’ (as cited by Anderson, 1987) to base his new concept on. Anderson (1987) incorporates the term ‘creep’ as defined by Greeley and Iverson (1985, as cited by Anderson 1987 and Zimbelman, Williams and Johnston, 2012) as part of his concept but uses it to define both large and well-sorted grains of sand. Further to this, the saltation chain reaction is inevitable as a grain will have a higher impact energy on landing than it does when the grain itself is ejected, therefore increasing the amount of saltating grains available, and inferring that it is saltation itself which is the main driver of sand transportation. It is shown by Werner and Haff (1987) that low-energy ejecta exhibits a monotonically kinetic energy increase, as the angle of incidence increases, as well as the impact energy increases. This is further proved by Willets and Rice's (1986) findings by employing high-speed photography to capture the movements and quantify saltation. They found the grains ricocheted off the surface at an angle greater than the impact angle in approximately two-thirds of the grains’ impact velocity. Werner and Haff (1986 and 1987) stated that with each individual saltating grain impact up to ten grains were ejected as a result, however, this ejection number is at its highest when the impact angle is close to 12 degrees. Anderson (1987 as cited by Zimbelman, Williams and Johnston, 2012) discusses how reptation is the main forming mechanism of ripples where “*initiation of sand ripples caused by small perturbations of the sand surface; perturbations grown by the influence of low-velocity grains ejected from the impact of high-velocity saltation grains*”.

Ripples reflect wind regime (Vaucher and Dashtgard, 2021), similarly as dunes do, however over much shorter timescales. Vaucher and Dashtgard (2021) state that the ripples morphology becomes more complex with depth in the ocean. Sinuous ripples on Earth indicate a low energy environment and therefore a slower sediment transport rate (Harms,

1969; Baas, 1994). Whereas linguoid ripples evidence a higher energy regime and so a higher transport rate of sediment (Baas, 1994). Grain size is thought to be influential on ripple size, whereas dune size is dependent on the flow regime and force (Bristow and Mountney, 2021; Richards, 1980).

Yizhaq *et al.,* (2020) tested Bagnold's concept along with considering Lapotre's (2016/2018) hypothesis, with particles sized 40 – 70 μm in a boundary layer wind tunnel. While also considering that both Bagnold, Greeley and Iversen (Yizhaq *et al.,* 2020) claimed that material was mostly transported by suspension or modified saltation therefore the 'reptation mechanism' (Anderson, 1987) being reduced. Yizhaq *et al.,* (2020) found the development and continual growth of ripples began with wind speeds of 3.6 m/s, where wavelengths and strength of sinuosity increased with increased wind speed, much like subaqueous ripples. An overlap where impact ripples and fluid drag ripples seem to coexist together is between wind speeds of 5 m/s and 6 m/s, where impact ripples are flattened at 6 m/s and the development of fluid drag ripples begin at 5 m/s. Flattening of the ripples occurred at a wind speed of 9.5 m/s. Importantly, their experiment found that impact ripples began to superimpose and form between fluid drag ripples when wind speed was reduced to 4 m/s which confirms that previous works of similar nature are all in agreement (Figure 2.5 and 2.6).

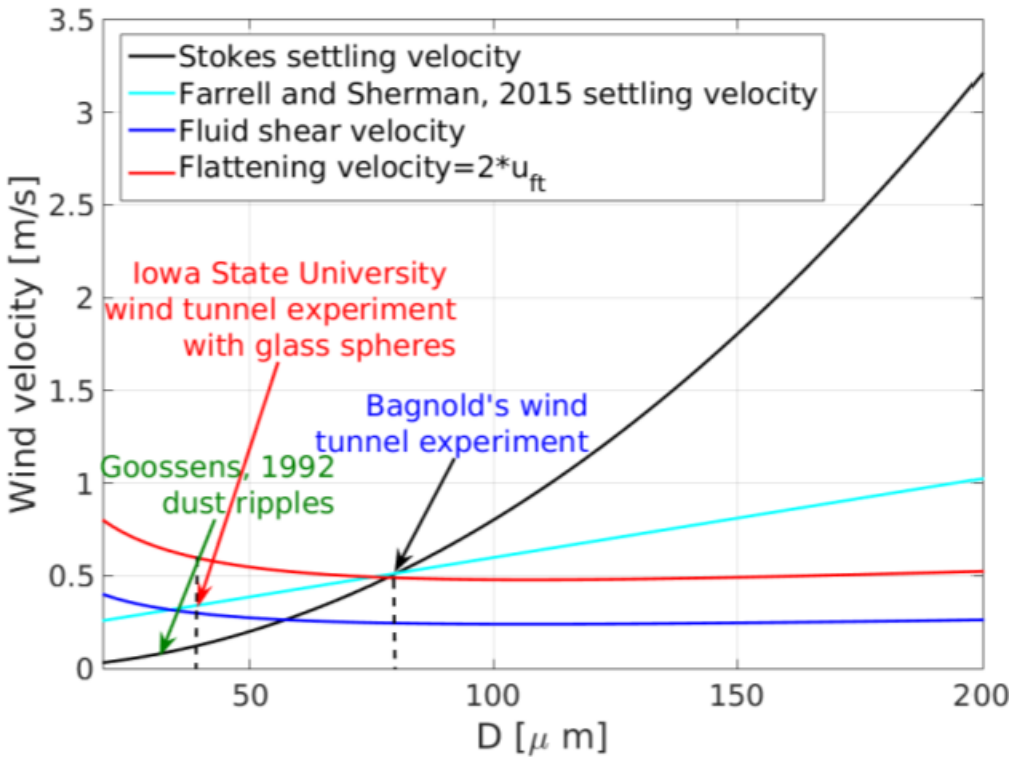

Figure 2.5 Sixth Planetary Dunes Workshop 2020 wind tunnel experiment (Yizhaq et al., 2020).

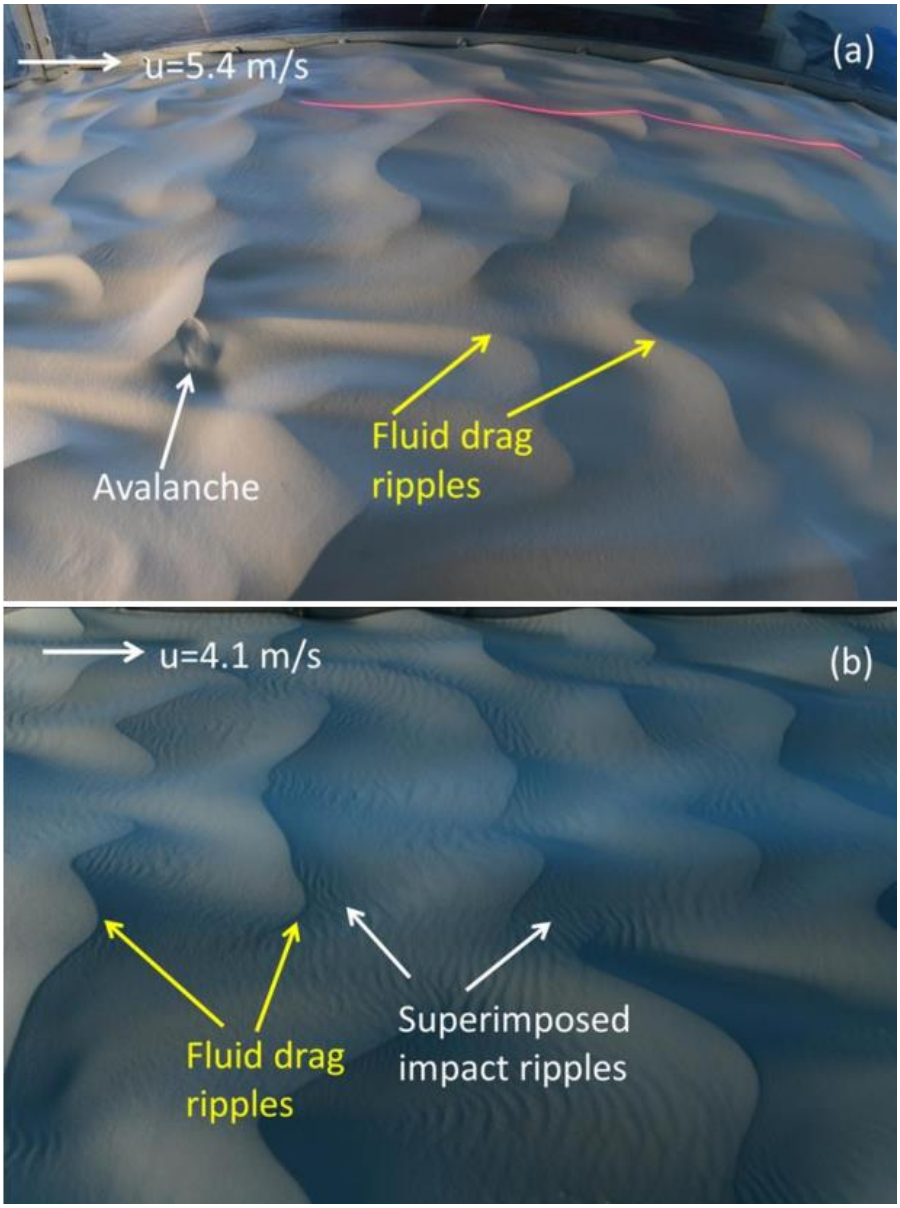

Figure 2.6 Wind tunnel experiment demonstrating the threshold overlap of the Fluid drag ripples and the superimposed ripples.

Large ripples on Mars are generally defined as having a wavelength between 1 and 5 m (mars.nasa.gov, 2016; Lapotre et al 2016; Day and Zimbelman, 2021, Silvestro et al 2016). Martian ripples require an even deeper understanding due to their morphological and formational complexity (reference). On Mars, ripples (Table 2.1) that are seen in satellite imagery must be at least in meter scale due to the present available spatial resolution, 25 cm

per pixel on the HiRISE imagery (2022). Any ripples smaller than this are not visible (Day and Zimbelman, 2021). However, evidence of smaller scale ripples has been pictured by rovers on Mars, having driven through decimetre to centimetre scale ripples (Day and Zimbelman, 2021; Diniega *et al.,* 2021). Martian ripple morphology is another grey area, as the official names for each type of ripple are still highly debated due to our lack of knowledge about ripple mechanics and how they should be divided into categories. However, Day and Zimbelman (2021) attempted to classify them, and this paper shall use these as guidelines for the geomorphic features on Mars.

Ripples on Earth have much smaller wavelengths and height of those seen on Mars (Yizhaq, Saban and Katra, 2020). Yizhaq, Saban and Katra (2020) found that there were two sizes of ripples found on Mars where there was no coarser grain armouring layer: small decimetre scale ripples and large meter-scale ripples. While the small-scale ripples can be directly compared to terrestrial analogues on Earth, the large ripples have no direct analogue, as they are smaller than the Martian megaripples coated in a layer of coarse grains which can be compared to Earths megaripples.

Large Martian ripples show a variety of characteristics that fall mostly into two types of ripples; impact ripples and fluid/wind drag ripples (Sullivan et al., 2020). Ripples that are found on Earth have been observed on Mars but on a much larger scale. However, the physics behind how some of these ripples are forming without the high-density liquid flow enabling them to form is not very well understood, of which is why Herschel crater's display of complex ripples are of much interest. Therefore, it is important to understand the physics behind how these ripples formed.

Table 2.1 Classification of ripples and dunes on Mars (Day and Zimbelman, 2021)

	Can be determined from orbital observations (except small ripples)			Sometimes determinable from orbital observations (except small ripples)		Requires surface observations	
	Plan view morphology	Size	Groups or solo	Dust cover (inferred)	Cross sectional morphology	Grain size	Surface stratification type
Small ripples	Straight-crested	cm-scale heights, cm-decimeter wavelengths	Groups, in sand patches or superimposed on larger bedforms	Absent	Symmetric or asymmetric	Any starting distribution	Reverse grading, wind ripple laminae
Large ripples	Straight-crested to sinuous	<1 m in height, m-scale spacing	Groups, in sand patches or superimposed on larger bedforms	Relatively low	Asymmetric	Fine-medium, unimodally distributed	Grainfall and some grainflow on lee faces as well as superimposed small ripples
Mega-ripples	Straight-crested to sinuous	<1 m in height, m-scale spacing	Mostly groups, but surface images suggest some form solo, uncommonly superimposed on larger bedforms	Usually relatively high	Symmetric or asymmetric	Coarse fraction present (by definition)	Grainfall, surface armoring of coarse grains
TARs	Straight-crested; rarely sinuous	>1 m height, >3 m- scale spacing	Groups of parallel bedforms	Relatively high	Symmetric	Not fully known, based on Dingo Gap: wide grain size distribution including coarse grains	Not well known on Mars
Dunes	Varied (barchan, star, linear, etc.; see Hayward et al., 2007)	>3 m height, decameter-km-spacing	Groups (fields) that may be widely spaced in regions with low sediment supply	Near absent for active dunes	Asymmetric (transverse) or symmetric (longitudinal)	Fine-medium, unimodally distributed	Cross stratified, combination of grainflow, grainfall, and wind ripple stratification

Impact ripples are those that from as a result of saltation (splash) like the aeolian ripples on Earth (Lapôtre, *et al.*, 2021; Sullivan et al., 2020). These ripples can be found superimposed on dunes or on sand sheets of which if the ripples are identified as indurated if they are covered by a layer of dust, or actively migrating and forming if they are dust free (Lapotre et al., 2018). Lapotre (2018) identified straight crested ripples on the lee slopes of dunes in the Namib desert and more sinuous crested ripples on the stoss slopes of the dunes. Which is consistent with evidence of the dynamics of impact ripples and gravitational forces creating a straight crest on the steep lee slopes (Lapotre et al., 2018). Lapotre *et al.,* (2018) further explains that where there are transverse ripples in a unidirectional flow regime, whether they be terrestrial wind drag ripples, large Martian ripples, coarse-grained ripples or current ripples, they all display sinuous crestlines. Wind-drag ripples on Mars are identified by their sinuous crest line and asymmetric profile much similar to those found under the influence of a current on Earth (Lapôtre, *et al.,* 2021).

The complexity of large Martian ripples can be further separated into bedform classes such as 2-D ripples and 3-D ripples. The 2-D ripples are found where there is a high sediment transport to a highly elevated dune, on longitudinal dune elements and/or on surfaces with gentle slopes (Silvestro *et al.,* 2016). Whereas 3-D ripples are more commonly found on lower dune elevations where there is poor sorting of sediment size and more complex and dynamic wind regimes (Pye and Tsoar, as cited by Silvestro *et al.,* 2016).

Yizhaq *et al.,* (2020) considers Lapotre *et al.,* (2016, 2018) hypothesis that large ripples are a result of fluid drag ripples when comparing its morphology to subaqueous ripples found on Earth. Lapotres *et al.,* (2016, 2018 as cited by Yizhaq *et al.*, 2020) state the similarity between

the sinuous crestlines of the Martian and Earths large ripples, the meter-scale mode of ripple wavelengths suggesting a more complex formative mechanism, and on the basis that there is a higher kinematic viscosity on Mars than on Earth supports his hypothesis and therefore are distinct from straight crested smaller wavelength impact ripples.

2.4 Dune shape influencing ripple morphology

A study carried out by Hood et al., (2012) studied how ripple patterns can explain the airflow across Martian dunes. Ripple patterns vary depending on their: orientation, wavelength, and rates of migration (Hood *et al.,* 2021). These are influenced by the local winds, topography (Hood *et al.,* 2021) and grain size (Wang, Zhang and Huang, 2019; Yizhaq and Katra, 2015; Zimbelman, Williams and Johnston, 2012) and this helps to understand the dynamics of air flow over the ripples and thus forth the dunes (Hood et al., 2012). Hood et al., (2012) found that the low-density atmosphere on Mars does not largely impact the behaviour of air flow over the differing topographies in the landscape.

Studying the wind flow over Mars using remote sensing equipment from the early studies using the Mariner 9 and Viking satellite flybys (Sullivan *et al.,* 2008; Edgett and Malin 2000) to the Mars Reconnaissance Orbiter (MRO) with the improved HiRISE imager aboard catching high resolution (up to 25 cm/pixel).

Baddock, Wiggs and Livingstone (2011) study found that airflow velocity is sustained before decelerating at the dune toe and increasing in velocity as it travels up the windward slope on a crest-brink separated dune. Airflow over dunes accelerates due to compression as the surface roughness decreases the shear stress when it travels up the stoss slope until it reaches the crest of the dune where the air flow travels down the lee slope and decompresses, therefore decelerates (Jackson and Hunt 1975; Bennet and Best 1995; Frank and Kocurek

1996; Baddock et al 2011; Smith et al 2017, as cited by Hood et al., 2021; Jerolmack et al., 2012 as cited by Runyon *et al.,* 2017). The airflow travelling over the crest brink decompresses due to being separated into a wake region (upper wake and lower wake), a reattachment point and a back-flow eddy circulation zone (Baddock, Livingstone and Wiggs, 2006) (Figure 2.7). An internal boundary layer (IBL) develops downwind of the reattatchment point where flow regains the overlying flow (Hood *et al.,* 2021) due to the increased surface roughness (Anderson and Chemacki, 2014 as cited by Runyon et al., 2017). The IBL layer broadens up into the atmosphere downwind due to the turbulent nature diffusing upwards which slows down the momentum of airflow (McLean and Smith, 1986 as cited by Runyon *et al.,* 2017). Another factor to consider is that with Mars atmosphere the Planetary Boundary Layer (PBL) can reach almost zero meters above the ground as the landscape surface heat capacity dramatically decreases during the nught (Runyon *et al.,* 2017). This, of course, is a simplified model and can vary depending on wind intensity and direction, the shape of the dune and the abundance and vicinity of the dune fields (Baddock *et al.,* 2011; Zgheib *et al.,* 2018a; Zgheib *et al.,* 2018 b; Bristow *et al.,* 2020 as cited by Hood *et al.,* 2021). In turn, the airflow over dunes also affects the dune shape as this controls the sedimentation transport process; migrating dunes upwind can collide with dunes downwind and the avalanching sediment on the leeward slope can create distinctive characteristics (Eastwood *et al.,* 2012; Swanson *et al.,* 2016; Bristow *et al.,* 2018; Lee *et al.,* 2019; Wang and Anderson, 2019; Assis and Franklin, 2020; Bacik *et al.,* 2020 as cited by Hood *et al.,* 2021) i.e., elongated horns.

Cardinale *et al.,* (2016) hypothesised that the PBL may be the main controlling factor for sand flux in Herschel Crater. According to Runyon *et al.,* (2017) the Global Circulation Models (GCM) for Herschel Crater and Nili Patera approximated that the free stream velocities 10 k

m are ~24-27 ms^{-1} of where the terrestrial value is 20 ms^{-1} at 1.9 km high for the White Sands study by (Jerolmack et al., 2012 as cited by Runyon et al., 2017).

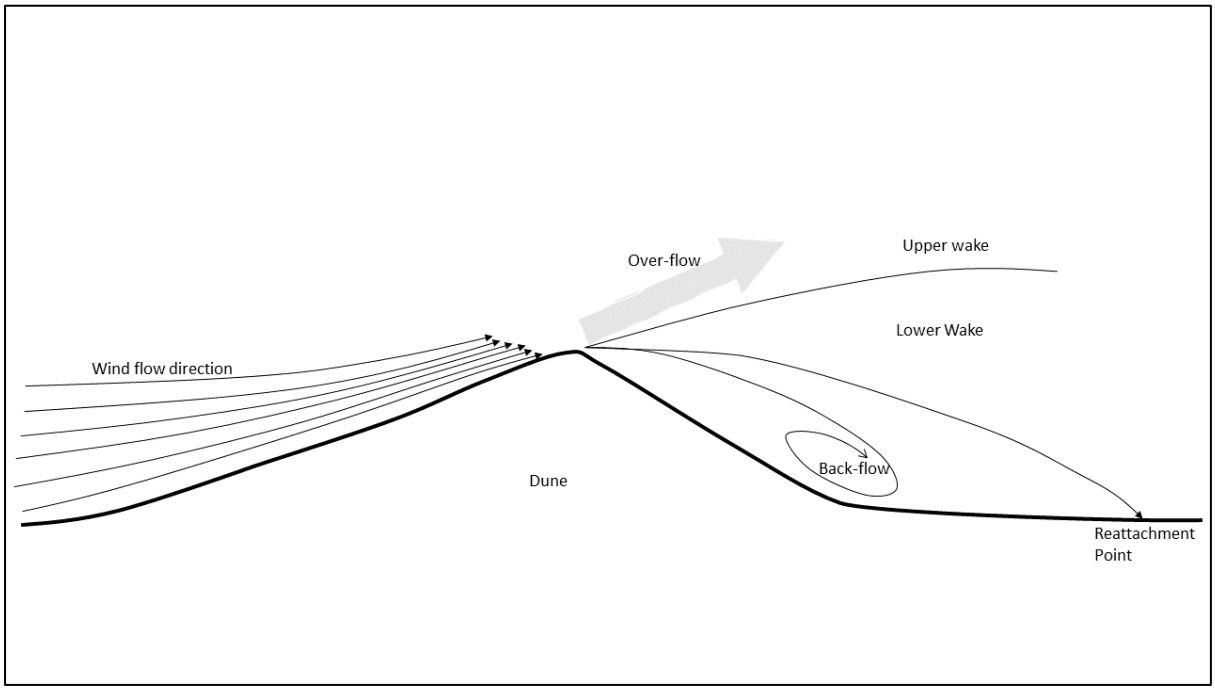

Figure 2.7 A schematic of dune morphology and airflow.

Airflow shapes the ripple patterns which have been identfied by Hood *et al.,* (2021) in Figure 2.7 This study found that the orientation of the ripples were as expected when related to the airflow over the dunes, with 2-D ripples on the dune flanks influenced by the dunes topography causing along-slope flow due to flow defelction, isotropic patterned ripples where the dune wake occurs and typical ripple patterns on the dune-top. Jackson *et al.,* (2012, as cited by Hood *et al.,* 2021) stated that ripple activity is majorly influenced by regional airflow of an area but local airflow that is strong enough to support sediment transport and the topography of the dune itself is what steers sediment flow.

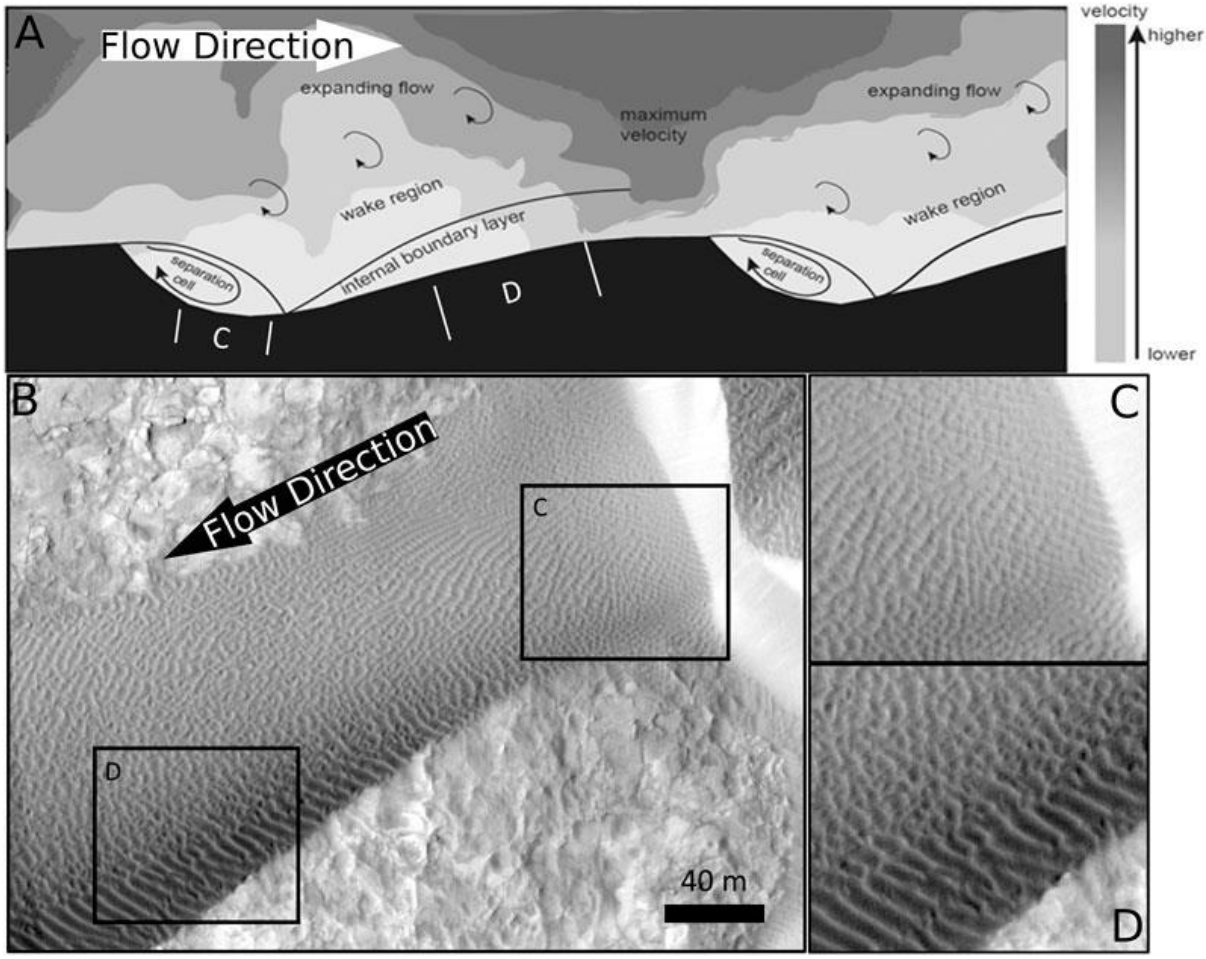

Figure 2.8 The airflow direction over dunes Hood et al 2021.

However, ripples can also represent seasonal cycles of airflow that do not necessarily represent the overall regional wind direction within the area; they don't always match with that of the inferred wind direction inferred from a dune's morphology (Jackson *et al.,* 2015; Silvestro *et al.,* 2016; Ewing *et al.,* 2017 as cited by Hood *et al.,* 2021).

On a flat surface, ripples are a very reliable and an easy way to assess the wind direction However, the relation between the inferred wind direction and orientation of the ripples is more complex when slope aspect is introduced as an additional factor. Martian dune flanks are usually populated with 2-D ripples and are generally deflected downslope in relation to

the slope gradient and aspect (Howard, 1977 as cited by Hood *et al.,* 2021) (Figure 2.7 to 2.9). Howards (1977) equation can be used to measure this:

$\sin(\beta) = (\tan(\theta) / \tan(\alpha)) \sin(\gamma)$

β – angle between wind direction and the ripple crest normal direction

θ – slope of the surface

γ – angle between wind direction and the slope aspect

α – angle of repose

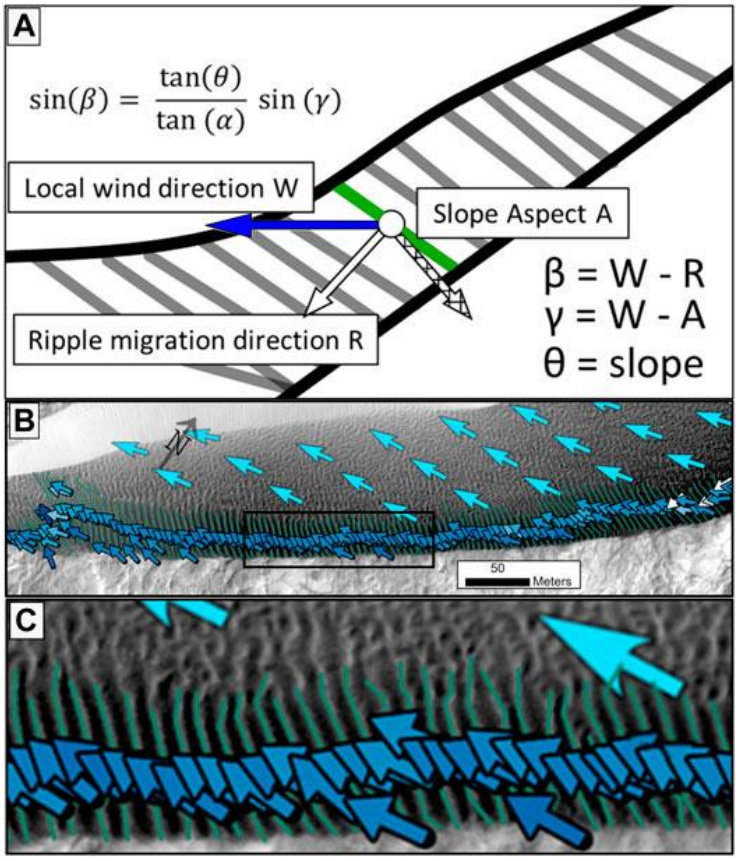

Figure 2.8 Howard equation which "predicts the deviation between formative wind direction and ripple orientation to scale with the deviation between the formative wind direction and

slope aspect modified by the ratio of the slope to the angle of repose" (A) and study site for Hood *et al.,* (2021).

Additionally, Howard's (1977) equation can be modified for Martian conditions, however while gravity and the density of the atmosphere on Mars is significantly different the angle of repose for Mars is very similar to that of Earth (Atwood-Stone and McEwen, 2013; Ewing *et al.,* 2017 as cited by Hood *et al.,* 2021).

An asymmetric feature, such as elongated horns, on barchan dunes are more likely to collide and interact with the stoss slope of dunes downwind. Adjacent dunes which each have elongated horns can collide together to form one single shared arm. Further collisions can occur off centre which merge the main bodies of the barchan dunes (Hood *et al.,* 2021). These collisions, interactions and linkage dunes can affect the dynamics of air flow over the dunes and therefore the ripple patterns (Hood *et al.,* 2021).

Hood's *et al.,* (2021) study found that where the slope gradient changes abruptly from steep on the dune flanks to the gently sloping stoss slope there was a very clear line of change between the 2-D ripples to 3-D ripples. However, the change was not so clearly defined where the transition is slope gradient was more gradual.

2.5 Herschel Crater Dunes

In both western and eastern Herschel crater there are large dune fields mainly composed of barchanoid dunes. Western Herschel crater studies show that the dominant wind regime trends north to south as evidenced from the ripples and dunes (Cardinale *et al,.* 2016). However, due to the asymmetric form of the barchan dunes and complexity of the superimposed ripples, Cardinale *et al.,* (2016) draws on Bagnolds *et al.,* (1941) research to

explain how a collision of multiple turbulent and variable winds may be influencing the sediment transport, bedform migration and therefore the airflow dynamics in the dune field. The strongest winds are evidenced to be adjacent to the crater rim where the dominant wind direction is irregular to that of the rest of the dune field, blowing west to east. The dunes were measured to be migrating an average rate of 0.2 metres per Earth year. Interestingly the ripple migration rates were so quick in the northern section of the dune field they were not trackable. However, the further towards the centre of the dune field the slower the ripples appear to migrate and therefore Cardinale *et al.,* (2016) was able to measure a migration rate of 0.3 metres per Earth year. Moreover, the rates of ripple migration were also variable depending on the dune hight where they migrated faster nearer to the crest of the dune. However according to (Davis *et al.,* 2019) dunes in Western Herschel Crater were measured to migrate approximately 0.3 meters per Earth Year southwest and are said to decelerate further downwind, based on 42 dunes.

Eastern Herschel crater dunes were measured to migrate at an average rate of 0.5 meters per Earth year towards the south southwest based off the 12 dunes in the upwind area of the dune field. It was evident that dune hight plays an influential role in sediment flux rates and therefore dune migration rates as the dunes on West Herschel crater were almost twice the hight of those in East Herschel crater (Davis *et al.,* 2019).

Dune height tends to be greater in east Herschel crater further upwind and are not found to form as much downwind when compared to dunes in west Herschel Crater. In west Herschel crater the dune height is not as high overall however the dune fields themselves are found further downwind. A negative correlation has been identified with dune height decreasing with increased distance downwind (Runyon *et al.,* 2017 and Bridges *et al.,* 2012).

Davis *et al.,* (2019) studies and previous HiRISE studies agree that migration rates are consistent with an average migration rate of 0.3/0.2 metres per Earth year. Interestingly

2.6 Central Herschel Dunes

Interestingly the dunes in Herschel crater were once identified as indurated (a solid relic feature) due to their apparently grooved texture in lower resolution imagery (Edgett and Malin, 2000b). This may have been due to the low-resolution imagery available at the time from the MOC, proving that that alone is not sufficient enough for modern day detailed research, but however is useful for bringing in evidence of topographical changes surrounding the dunes themselves. It is only since the return of the HiRISE imagery since 2006 which has enabled the detailed study of these dunes with their superimposed ripples, tracking their active migration over a series of timestamped satellite photos. The complexity of sinuous longitudinal ripples superimposed on dunes are found in Herschel Crater pictured by HiRISE 2010 to 2017. Herschel Crater itself is located in the Terra Cimmeria region of Mars (14°S, 129°W) situated near the boundary of the southern highlands and northern lowlands (HiRISE, 2022). Some of the dune fields in Herschel have been researched however the area of particular interest has yet to be studied in depth.

Present-day aeolian activity in Herschel Crater has been researched (Runyon *et al.,* 2017; Cardinale *et al.,* 2016) but the studies have focused on the western, eastern, and southern areas of the crater. Cardinale *et al.,* (2016) notes that there are complex ripples present on the stoss slopes of the barchan dunes in their study area (western side of the crater), as seen in this thesis's study area. There are multiple influences on dune and ripple formation which include: topography (Figure 2.9), crater floor roughness, sediment supply, sediment type,

wind regime and wind velocity (Bourke, 2004; Chojnacki *et al.,* 2019). The Herschel Crater basin is regarded as Noachian in age and comprises three landforms: mountainous remnants of the central peak and peak rim, hilly and texturally rough basin floor and a wrinkle-ridge plain (Edgett, 1991) (Figure 2.2). The majority of sediment (thought to be sand) indicated by dark patches dominantly found in the southern areas of the crater indicate a dominant wind direction from the north (Edgett, 1991). However, Edgett (1991) states that evidence of yardang erosion indicates a palaeowind direction from the west.

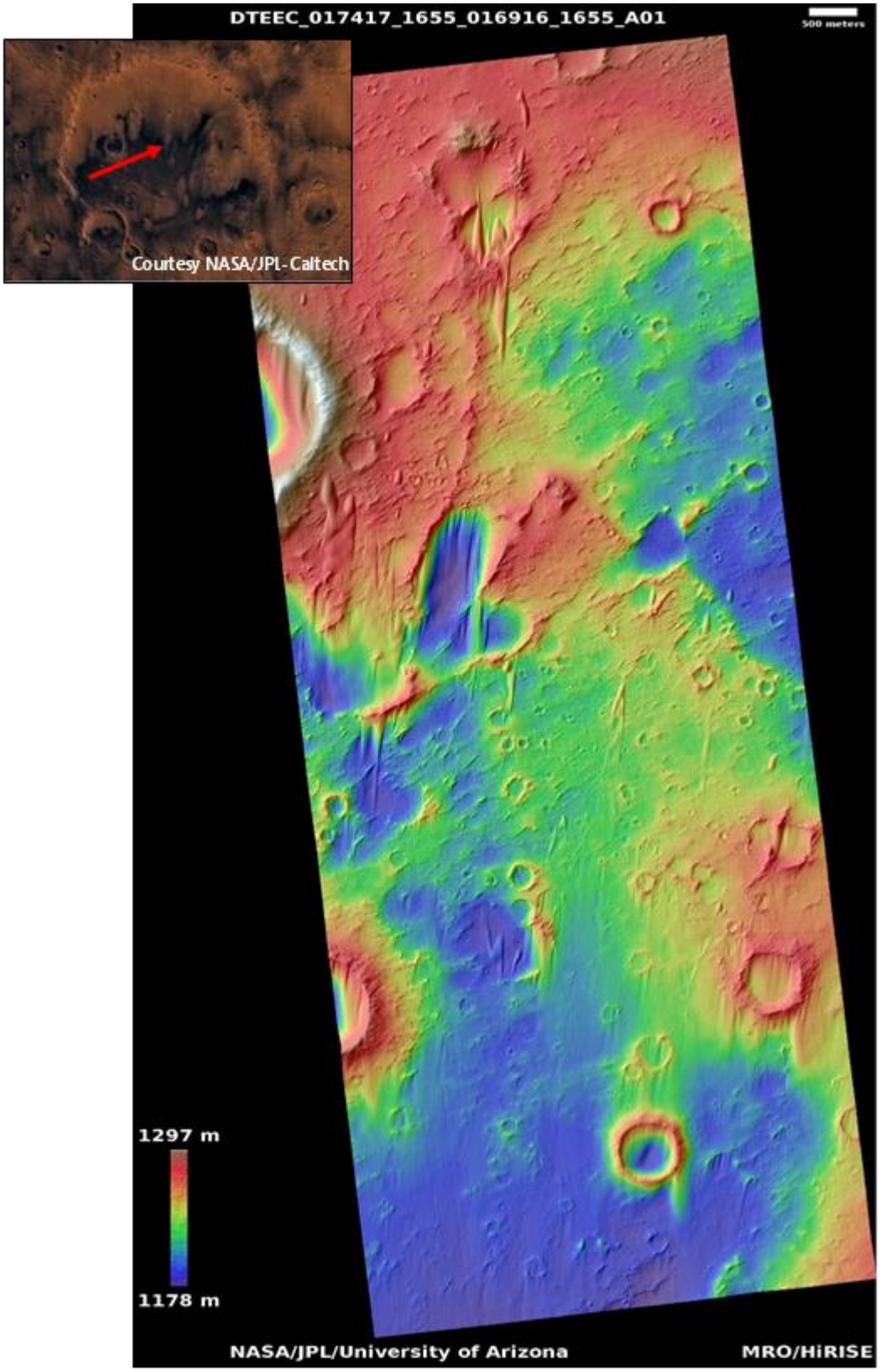

Figure 2.9 The Digital Elevation Model for the study area in Herschel Crater (NASA/JPL/UArizona).

The Digital Elevation Model for the study area in Herschel Crater (NASA/JPL/UArizona).

3. Methodology

This chapter describes and outlines the study area and the methods for automated ripple crestline detection and migration with reference to the Central Herschel Crater, Mars. This chapter will then in turn address the following areas: data sources utilised, the GIS procedure and the statistical analysis methods applied to the outputs generated. This methodology uses a modified version of crestline detection GIS techniques developed by Telfer *et al,* (2015), applied to detect the crestlines of dunes on Mars. The methods for the analytical processes developed for this thesis have been undertaken using ArcGIS Pro 2.9.5 and the programming language R. These will be described in turn within this chapter.

3.1 Study Area

Herschel Crater, latitude -14° longitude 129°, is one of the craters that is a Noachian impact basin within the Mare Tyrrenium region (Cardinale *et al.,* 2016) in the southern hemisphere of Mars. The once thought indurated dunes (Edgett and Malin, 2000) have been proven since to show recent activity (Bridges *et al.,* 2007) in both western and eastern Herschel Crater (Cardinale *et al.,* 2016). However, no activity has been studied in central Herschel where there are isolated barchan dunes present. The ripples that show complex patterns have been otherwise dismissed as no more than a 'complex ripple' (Cardinale *et al.,* 2016; Bridges, 2013; Edgett and Malin, 2000) in other parts of Herschel crater, and the isolated dunes themselves are thought to be moving at similar rates to that on the west and east portions of the crater. However, at the time of writing there are no published papers that have addressed how much these large sinusoidal (complex) ripples found on the back of the dune and the large straight crested transverse ripples on the dune flanks have migrated, the average rates of their migration or why they may be so complex. The airflow dynamics and migration pattern behind

the formation of these ripples could contribute a deeper understanding to Mars's atmosphere, past and present wind regime and could enhance the knowledge of its climate.

3.2 Data sources and overview

Figure 3.1 provides an analytical overview of the processes is found within this chapter. It is broken down into two workflows concerning the data preparation, analysis and outputs using GIS (see Section 3.3) and the evaluation of the outputs (crestlines and migration rates) using R (see Section 3.6).

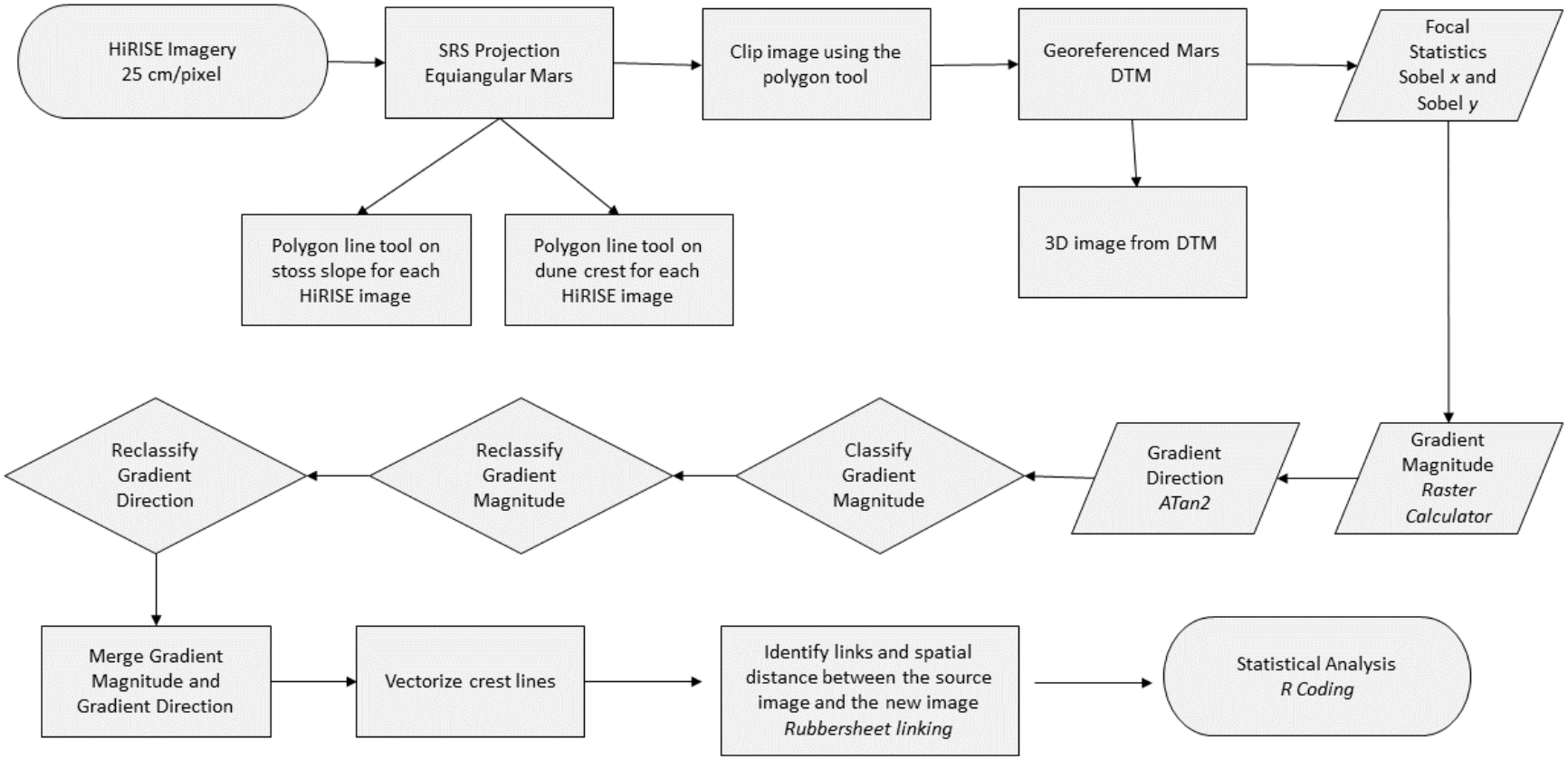

Figure 3.1 Summation of analytical procedures for ripple and dune migration assessment in central Herschel Crater.

High resolution DTMs for Mars were obtained from HiRISE (2022). For optimal results of bedform migration and analysis these were deemed the best suited for this study, Herschel Crater, due to its high spatial-resolution (25 cm/pixel) enabling <1 m features to be resolved. For the best possible results, good illumination and full resolution of the images are preferred, however with limited data available for this study site all images (2010-2017) were used (Table 4.1).

Table 3.1 Mars satellite imagery data sources used. Source: HiRISE (2022)

Image Number	File Number	Acquisition Date	Latitude (centred)	Longitude (East)	Spacecraft Altitude (miles)
1	ESP_016916_1655	06 March 2010	-14.104°	129.687°	161.3
2	ESP_017417_1655	14 April 2010	-14.135°	129.688°	161.4
3	ESP_025487_1655	03 January 2012	-14.138°	129.701°	161.4
4	ESP_043157_1655	11 October 2015	-14.106°	129.688°	161.4
5	ESP_053218_1655	03 December 2017	-14.098°	129.687°	161.5

3.3 GIS and DTM data pre-processing

The DTM for this study were pre-processed using ArcGIS Pro 2.9.5 (Figure 2.9). Firstly, the DTM data for the five different dates (Table 4.1) were clipped to the study area. A polygon was created to outline the study area and used to clip the DTM.

The clipped DTMs were georeferenced through adding a minimum of three control points in the raster dataset that links the overlaying image to the original image ESP_016916_1655 (Image Number 1, Table 4.1). The control points used to link the images are fixed to permanent features within all imagery, such as crater rims. The coordinate reference system 'Mars Equiangular' was used to correctly geolocate the DTMs on the surface.

3.4 Ripple Crestline Detection

To create crestlines that lined the ridges of the ripples superimposed on the barchan dune, a modified version of Telfers *et al.'s,* (2015) crestline detection algorithm was used. It is essential to automate feature identification due to the volume of data being used, geographical extent of the study site and scalability for future Mars research.

The following methodology describes the approach taken for automated crestline detection. In order to detect a crestline its prominence over surrounding features based on cell height, slope and aspect are required. In order to achieve this, firstly, the Focal Statistics (Figure 4.1) tool was used to calculate the cell input of intersecting neighbourhoods.

This tool calculates a chosen statistic for a given cell, based on a window (kernel) around it (Figure 4.2).

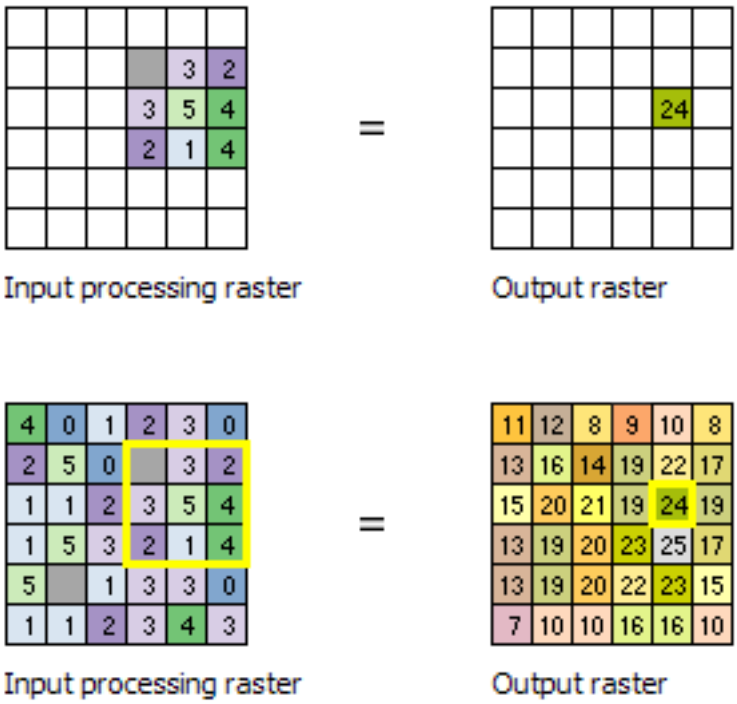

figure 4.2 Schematic for the application of focal statistics for raster (DTM) cell (ESRI, 2022).

The neighbourhoods were weighted to a specified kernel file. Next the Convolution Function was applied which filtered the pixel values through calculating the pixel values based on the weights of the neighbours based on the kernel applied. This results in a crestline raster output, sharpening the image so that the crestlines are defined clearly for use in subsequent analyses.

The crestline gradient magnitude and gradient direction were calculated using the Raster Calculator (Figure 4.1). To generate a gradient direction and magnitude of the crestlines the map algebraic equation was used.

The Reclassify tool was applied to the gradient magnitude and direction to change the cell values so that they had a common scale of values.

3.5 Automated crestline detection

The methodology so far has produced sets of dune crestlines for each timestamped satellite image. An aim of this thesis is to detect dune and ripple migration. In principle this can be achieved through a manual visual analysis by identifying corresponding crestlines at different times, measuring them next to a fixed object (e.g. boulder or crater rim). However, this is not practical or feasible over a large temporal and spatial scale. GIS can be used to automate this task. The ArcGIS Pro *Generate Rubbersheet Links (Editing)* tool in the conflation toolset links line features from different data sources covering the same area (ESRI, 2023). This tool identifies matching nodes on corresponding line features. This is of particular relevance for detecting the spatial offset between dune crestlines observed at different dates. It generates an output feature consisting of pairs of nodes, the movement direction and length (distance) between the nodes (i.e. the rubbersheet links). Figure 3.2 shows a schematic overview of this process.

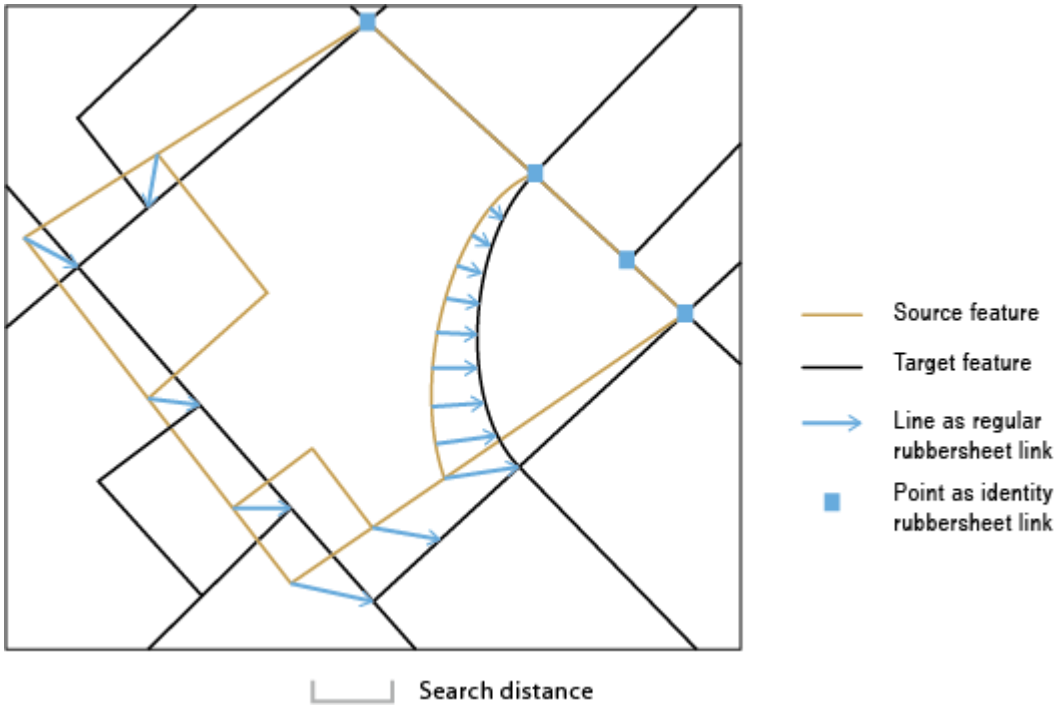

Figure 3.2 Rubbersheet linking matching the target line feature to the corresponding source feature location (ESRI, 2023).

The input parameters of this tool consist of the two sets of crestlines at different dates (the source and target lines) and a search distance (shown in grey in Figure 3.2). The outputs of this tool quantifying crestline migration are heavily dependent on the search distance parameter. The search distance is the window used to detect matching pairs of nodes on corresponding crestlines. This needs to be set at a small enough value to capture the migration of the crestlines. If this is set too large it can result in misidentification of crestline node pairs and unnecessarily increase computational processing demands. Crestline migration can be variable within the same location. With this in mind a sensitivity analysis was undertaken to examine the best match between nodes and assess migration distance by running the tool at 1 m, 2 m and 4 m search distance. This were visually and statistically analysed (see Section X). The initial search distance was based on visual observation of the data which show ripple crestlines moving approximately >0 to 1.5 m over the duration of this

study. For this study, and following the sensitivity analysis results (Section 4.3) a 2 m Rubbersheet Link search distance parameter was accepted as the most appropriate for analyses.

3.6 R statistical Analysis

A statistical analysis was undertaken to examine the difference in ripple crestline migration distance outputs from the Rubbersheet Links analysis. For this, two corresponding sets of crestlines node links were used for the dates 06 March 2010 to 14 April 2010 (images 1 and 2, Table 3.1). These were kept the same in the sensitivity analysis, with only the search distance parameter being varied each time. The Rubbersheet Link analysis using these same inputs was repeated with a varied search distance parameter set to 1 m, 3 m and 4 m. These data, a table of pairs of nodes and distances between them, were exported from ArcGIS Pro as CSV format and analysed using the programming language R in R Studio (Appendix A). Firstly, a Shapiro normality test was carried out using the `shapiro.test()` function. These data sets were not normally distributed ($p > 0.05$). Therefore, the Wilcoxon Mann Whitney U (`wilcox.test()`) non-parametric test for difference was used to examine whether a statistically significant ($\alpha = 0.05$) difference existed between analyses undertaken using the different search distance parameters.

3.7 MRO image compilation

Due to the complexity of the geomorphology displayed on Herschel Crater, and to gain the bigger picture, can help determine factors such as sediment supply, and airflow defects from topography that can influence wind regimes and sediment transport. To achieve this, images from the MRO Context Camera was used to create a wide-angle picture of central Herschel Crater.

Table 3.2 Crestline Detection periods for each group.

Group	Detection period
1	06 March 2010 to 14 April 2010
2	14 April 2010 to 03 January 2012
3	03 January 2012 to 11 October 2015
4	11 October 2015 to 03 December 2017

4. Results

This chapter presents the results from the methodology. Firstly, it presents the study area and wider region for context. This is followed by the detection of the dune migration rates and then the ripple crestline detection and migration rates. The final subchapter presents results of the automated ripple crestline detection procedure and analysis of these rates.

4.1 Regional Context imagery

Using the Context Camera on NASA's Mars Reconnaissance Orbiter (MRO) images were added into the ESRI ArcGIS Pro programme to enable a wider region view (Figure 4.1). The dunes found in central Herschel Crater are part of the most northerly dunes until reaching the rims of the crater in the east and west. The dune studied in Herschel Crater consist of a sediment availability-limited asymmetric barchan with an elongated eastern horn. The dune is isolated and is migrating along bedrock. Downwind (south) of the dune are sand sheets. The ripples superimposed on the dunes are also found on these sand sheets of Herschel Crater. North of the central Herschel Crater dunes is a flat/gently dipping rough (heavily cratered) topography. A ridge is shown halfway between the dune itself and the northern edge of the crater. The image clearly evidence that the southern portion of the crater is a far more rough and rigid landscape with fewer dunes rough than the northern portion as there are topographical highs and lows easily visible. Furthermore, its distinctly shows darker streaks of material swept in a southerly direction, its source starting at the dunes in Herschel Crater. This indicates that the majority of sediment transport in this crater is sourced from the dunes themselves rather than surrounding weathering and erosion of bedrock. The sweeping direction of the sediment appears to be almost directly south in the centre of the crater whereas the eastern portion of the crater shows a more south-westerly direction of transport.

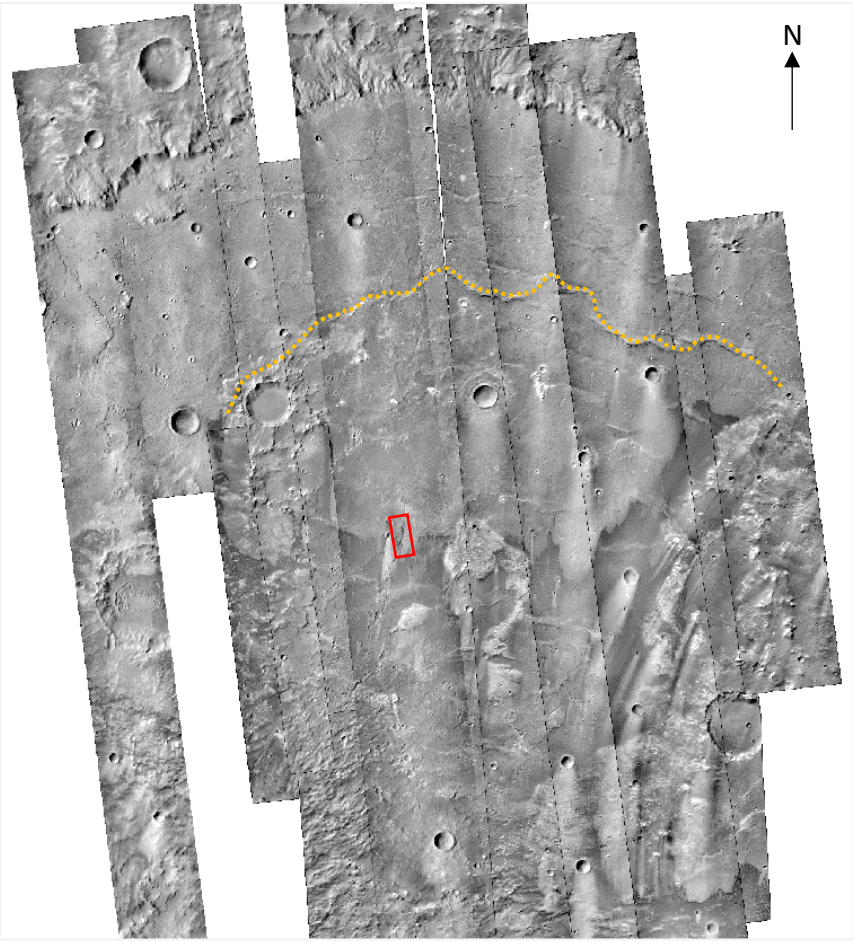

Figure 4.1 A combination of MRO Context Images from HiRISE in ESRI ArcGIS Pro. The study area is outlined by a red box. The ridge is indicated by the dashed yellow line north of the study area. Image: NASA/JPL/University of Arizona.

4.2 Dune migration rates

Detection of dune migration was conducted by simple georeferencing of images collected from HiRISE 2010 to 2017 of central Herschel Crater which was input into ESRI ArcGIS Pro. The barchan has a stoss slope and slipe face and an elongated easterly horn which thickens midway downwind before thinning again. A primary visual analysis of the dune immediately shows the base (upwind) of the stoss slope is migrating southwards (Figure 4.1), indicating a northerly wind. The elongated horn also shows migration of material southwards.

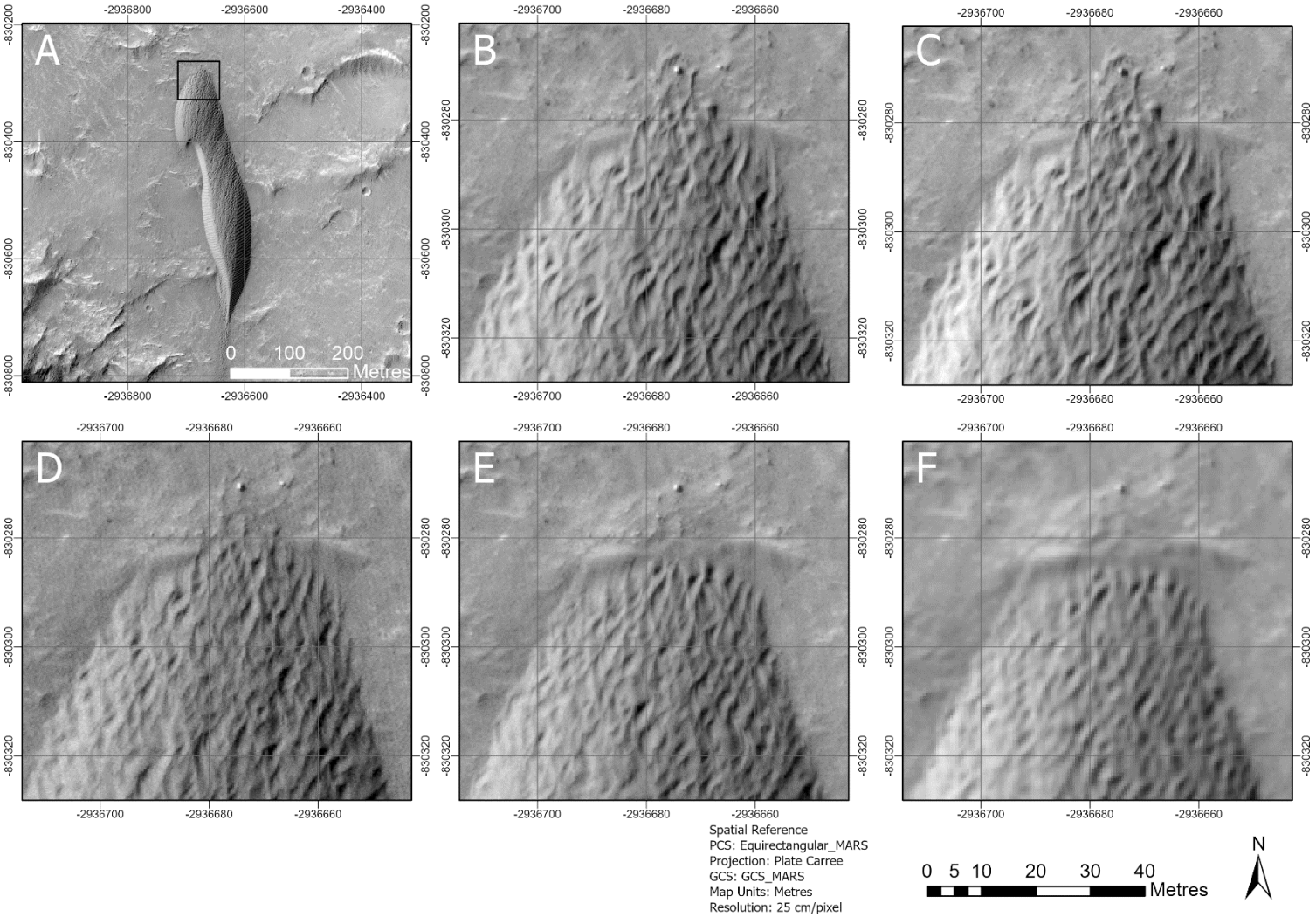

Figure 4.2 A: An overview map of the Central Herschel study area showing the extent indicator (black outline) for large scale dune migration overviews B-F. B-F: dune stoss edge on 06 March 2010, 14 April 2010, 03 January 2012, 11 October 2015 and 03 December 2017.

The largest distance measured in ArcGIS Pro at the back of the stoss slope was 7.2 m over a 1 year and 8-month period. This was between C – D in Figure 4.2 (Images 2 and 3, see Table 3.1). This would calculate as an average migration distance of up to 4.2 m per year. The distance measured was from a fixed feature, appearing as a boulder just north of the dune, and the last ripple related to the dune. The slip face of the barchan has shown southward migration of 9.70 m overall (Figure 4.4).

4.3 Ripple Crestline detection and migration rates

Using a modified version of Telfer *et al.,* (2015) algorithm for crest detection of ripples superimposed on dunes in Central Herschel Crater in ESRI ArcGIS Pro, analysis was conducted on the HiRISE images compiled from 2010 to 2017.

Martian large ripples superimposed on the dune show prevalent migration, however the direction of migration is inconsistent which each time framed image (Figures 4.5 to 4.7). As a whole, the trend of the ripple crestlines reflect bidirectional wind regime. Two groups of ripples were identified within the study are 2-D ripples present of the flanks of the dune and 3-D ripples present on the stoss (windward) slope of the dune. The 3-D stoss slope ripples present sinuosity, lunate and lobe features highly changeable between each time image making it almost impossible to track with or without the ESRI ArcGIS Pro algorithm. These complex 3-D ripple patterns superimposed on dunes and sand sheets are generally found for ~90% of the study area in Central Herschel Crater. The 2-D ripples are straight crested linear ripples with junctions and imperfections presented, however the ripple junctions are smoothed out on the western flank of the elongated horn of the barchan dune after the year 2012, while the eastern flank remains to have imperfections throughout.

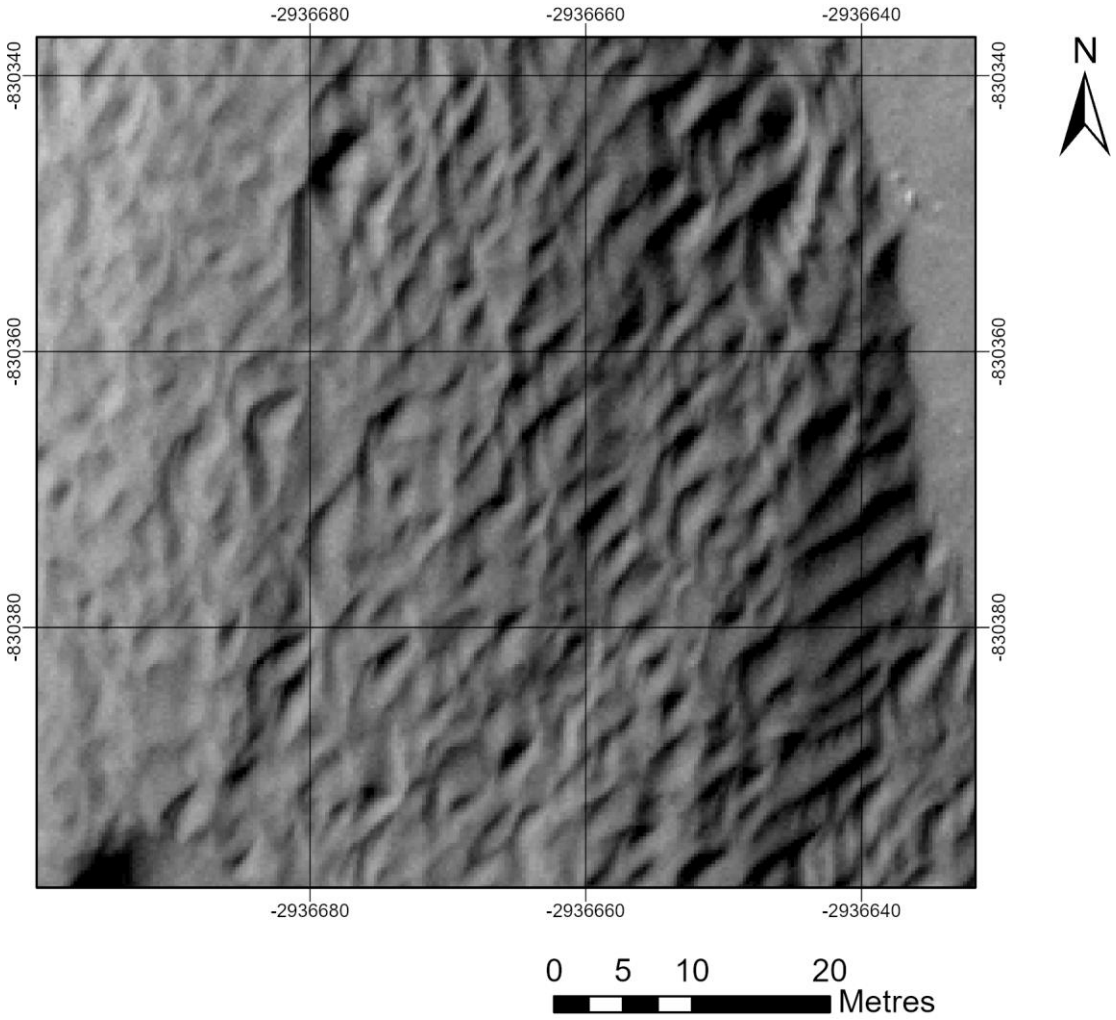

Figure 4.3 Caption complex 3-D ripples superimposed on the stoss slope and 2-D ripples on the flank of the barchan dune. Image: NASA/JPL/University of Arizona.

The slip face of the barchan dune migrates southwards however morphologically it changes shape between the time frames of 2012 and 2015. In 2012, and prior to, it shows a straight edges crestline whereas in 2015 and 2017 the 3-D ripples superimposed on the stoss slope of the dune begin to develop down the slip face (Figure 4.4).

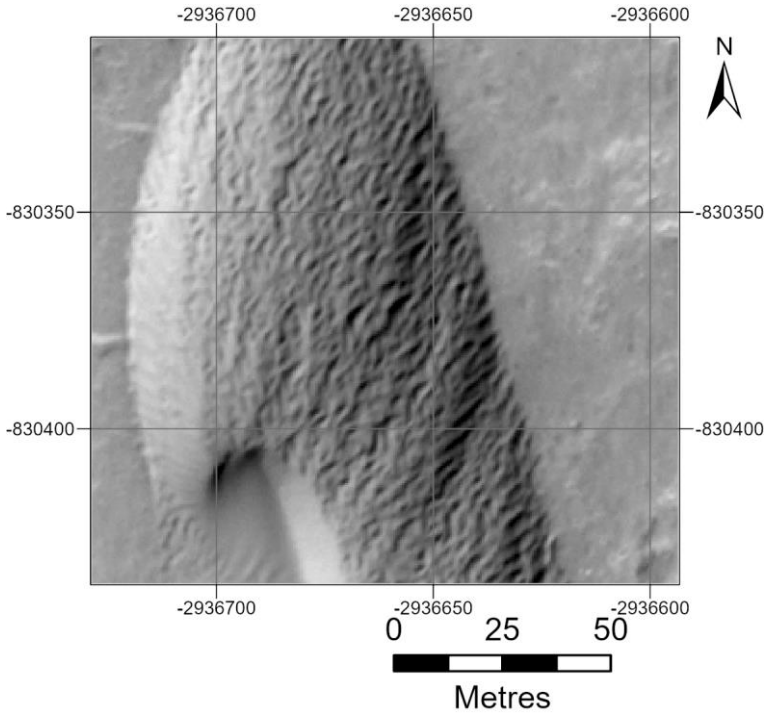

Figure 4.4 Slip face of the barchan dune with A) evidencing a straight crestline in 2012 and B) evidencing the 3-D complex ripples superimposed on the stoss slope beginning to migration and develop down on the slip face in 2015.

Analysis of the ripples show that the ripples are active from the crestline detection algorithm. However, due to the nature of the complex ripples it made it increasingly difficult to find a migratory pattern and direction (Figure 4.2). Analysis was carried out by firstly studying year by year for each image (Figure 4.2) and then by a final first image and last image from HiRISE.

Using the Rubber sheet linking tool, it joined nodes of the matching crestlines in each time frames which allowed for a distance to be automatically and accurately measured. From this the distances were put into the programme R and the mean, median standard deviation (SD) and the Coefficient Variation (CV) was calculated (Table 4.1).

Table 4.1 Crestline migration rate statistics (2 m search distance parameter), summarised using R, for the Herschel Crater dune.

Date	Calculated Crestline Migration (metres)			CV
	Mean	Median	SD	
March 2010 - 2010	1.11	1.02	0.67	0.60
2010-2012	1.04	0.93	0.66	0.64
2012-2015	1.08	0.98	0.66	0.61
2015-2017	1.11	1.02	0.67	0.60

In Figure 4.5 to 4.7 it shows the crest line ripples on the dune individually and combined for analysis of ripple displacement. Figure 4.5 to 4.7 reveals that small movement occurred across the study area and evidence of migration northward from the 2-D straight crested ripples on the dune flanks was present between March 2010 and April 2010.

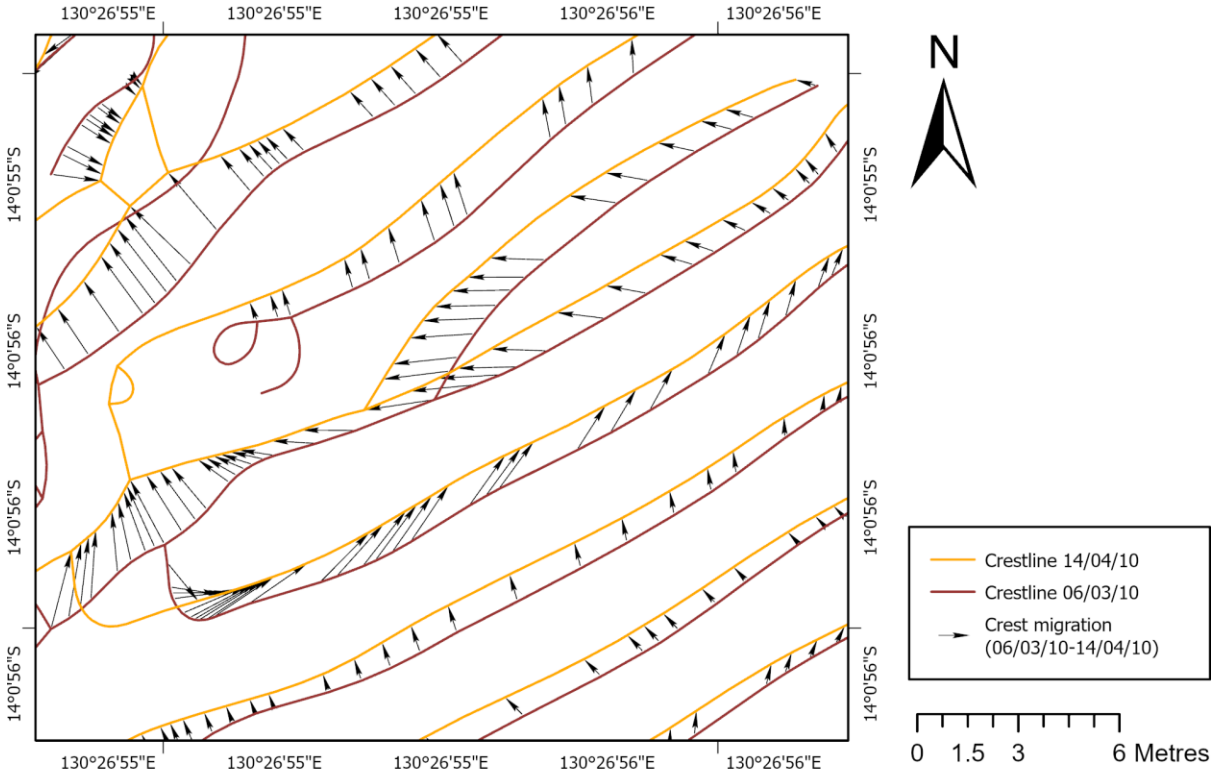

Figure 4.5 The 2 m search distance parameter for Rubbersheet Link between the straight crested ripple crestlines on the dune flanks for 06/03/2010 and 14/04/2010.

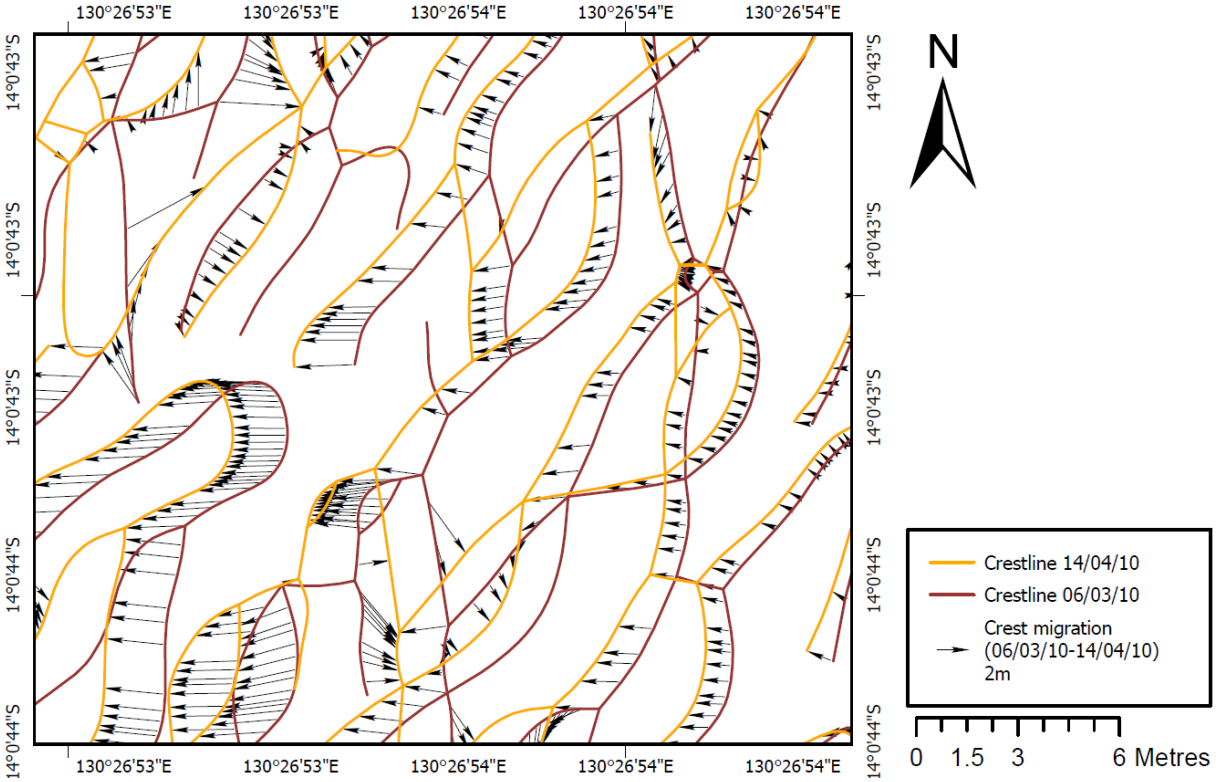

Figure 4.6 The 2 m search distance parameter for Rubbersheet Link between the sinusiodal complex crestlines on the dune stoss slope for 06/03/2010 to 14/04/2010.

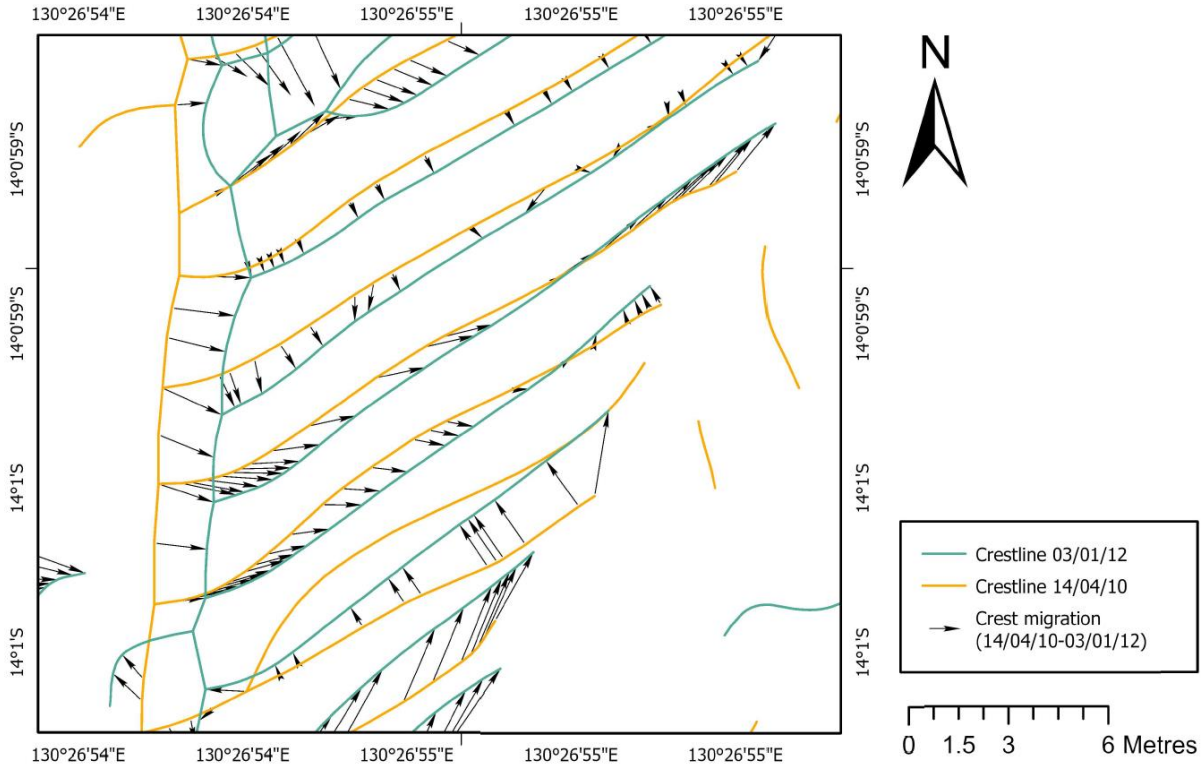

Figure 4.7 The 2 m search distance parameter for Rubbersheet Link between the straight crested crestlines on the dune flanks between 06/03/2010 and 14/04/2010.

Table 4.2 Average ripple migration rate from rubbersheet link analysis using the mean migration distance measurements.

Group No.	Average Migration Distance (metres)	Time frame (years)	Average Migration Rate (m/year)
1	1.11	0.11	0.12
2	1.04	1.7	0.61
3	1.08	3.7	0.29
4	1.11	2.1	0.53

The average migration rate for these ripples varied from 0.12 m in Group 1 to 0.61 m per year in Group 2 (Table 4.2). Therefore, the overall average migration rate for these ripples over the time framed images (Group 1 – 4) is 0.38 m per earth year.

4.4 Statistical sensitivity analysis

A statistical sensitivity analysis of the impact of the search distance parameter of the Rubbersheet Link tool was undertaken to assess the effect on migration rates and select an appropriate value for the subsequent analyses (Section 3.5). A mean, median, standard deviation (SD) and coefficient of variation (CV) was calculated in R for the crestline migration rates from the Rubbersheet Linking tool on ArcGIS Pro 2.9.5 (2022) between the timestamped images of the study area. Descriptive statistics for migration rates based on the different search distance parameters are shown in Table 4.3. The largest impact on the mean and median crestline migration occurs when comparing the difference between the 1 m and 3 m search distance parameter setting, even though the rest of the inputs were the same. However, the greatest variation relative to the mean is observed for the 4 m search distance setting (CV = 0.794, Table 4.3, Figure 4.2).

Table 4.3 ArcGIS Pro Rubbersheet Link calculated crestline migration statistics, summarised using R, for different search distance parameters.

Search Distance Parameter	**Calculated Crestline Migration (metres)**			**CV**
	Mean	**Median**	**SD**	
1 metre	0.547	0.487	0.329	0.602
3 metre	1.127	0.894	0.840	0.745
4 metre	1.327	1.021	1.054	0.794

Note: the time period to detect crestline change was kept constant (date 1 input: 06/03/2010, date 2: 14/04/2010) with only the search distance (column 1) changed each time.

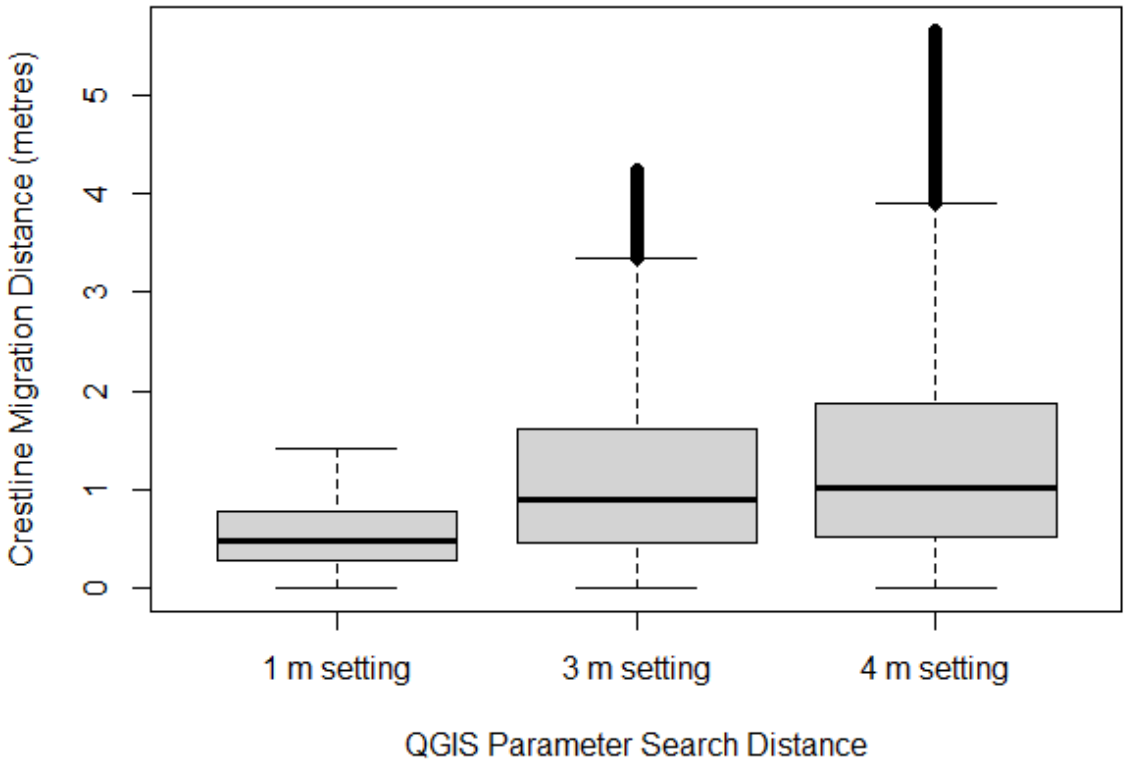

Figure 4.8 Boxplot of the crestline migration between matching nodes for 1, 3 and 4 m search distance parameters.

Using R, the difference on migration rates caused by the search distance parameter was statistically examined. The Shapiro test proved the data were not normally distributed ($p < 2.2e\text{-}16$), therefore, the Wilcoxon test was carried out (Table x). The following hypotheses were established:

- Null hypothesis (H0): There is no difference in migration distance results between 1m and 3m parameter settings.
- Alternative hypothesis (H1): There is a difference in migration distance results between 1m and 3m parameter settings.

Table 4.4 Wilcoxon Statistical Test for difference results using 1 m, 3 m and 4 m crestline migration search distance parameters.

Test Scenario	p-value	W (test statistic)
1 m vs 3 m	< 0.0001	88798449
3 m vs 4 m	< 0.0001	197638614

The null hypothesis can be rejected as the P-value is less than 0.05. There is a significant difference in migration distance results between 1 m versus 3 m parameter and 3 m versus 4 m settings with a 95% confidence. However, the test statistics are similar in that they are both very large (Table 4.4.). This suggests that the high and low ranks are fairly even distributed between the two scenarios. This could be interpreted as both of the outputs producing a fairly even number of both high and low migration rates between matching nodes. For the subsequent analyses a 2 m search distance parameter was chosen. This is because the results presented here show that 1 m was too small to detect pairs of matching nodes, as migration rates exceeded this, while 3 and 4 m was too high (Table 4.4). A search distance parameter too high results in the misidentification of node pairs by overextending the search window, linking out of phase crestlines (see Section 3.4; ESRI, 2023).

5. Discussion

This chapter discusses the results and how these have been inferred to understand the complexity of the dune and ripple migration and morphology using the literature in Chapter 2.

5.1 Regional Context Imagery

Herschel Crater is located in the southern highlands of Mars. Imagery from HiRISE (2022) was stitched together so that a regional assessment of the crater could be carried out and used in inferring how this could be influencing wind regime and thus the dune and ripple migration rates and their complexity. In Figure 4.1 the darker streaks of material swept in a southerly and south-westerly direction, indicates the sediment source is from the dunes themselves instead than weathering and erosion of surrounding bedrock. The sweeping direction of the sediment appears to be almost directly south in the centre of the crater whereas the eastern portion of the crater shows a more south-westerly direction of transport. This would imply the wind direction varies within the crater and subsequently causes a more complex wind regime directly impacted from the topography of the crater, the crater floor and perhaps even the dunes themselves (Cardinale *et al.,* 2012). Additionally, the ridge shown halfway between the study dune and the northern crater rim could influence wind patterns in the crater. As the study dune is the most northly dune found in central Herschel Crater, it could be exposed to very turbulent wind patterns compared to those that are found further south. The southern portion of the crater shows a more rough and rigid landscape with fewer dunes suggesting dunes are not able to grow or initiate in the southern portion.

5.2 Study dune in Herschel Crater

This site evidence barchan dunes made of limited sediment availability, as proven by the elongated horn, its position directly on bedrock and its isolation from other dunes along with the assessment of sediment transport described in chapter 5.1. From the low-resolution MRO imagery, the dune in central Herschel Crater showed undulating features on the stoss slope (Figure 4.2), which was argued that this was evidence of induration of the dune (Bridges 2010; Edgett, Kenneth and Malin, 2000). The indurated theory was discounted when higher resolution imagery was aquired from HiRISE became available for the study area in 2010, evidencing that the dune was in fact an active dune (Cardinale *et al.,* 2016). However, the dune itself does show an undulation on its stoss slope and could be interpreted as indications of the collision or linkage of two dunes (Hersen and Douady, 2005). Therefore, it is quite possible that there were two barchan dunes once present in this location. Due to the undulation occurring on the stoss slope up until where the elongated horn of the barchan occurs it could be inferred that the elongated horn of the upwind dune collided with a downwind barchan or linear dune to create one barchan dune with a very elongated horn.

5.3 Dune Migration

Migration of the dune is clearly visible between images 1 to 5 (see Table 3.1 and Figure 4.2). Upon visual analysis of the dune migration, it appears that the migration of the dune is at its most between 2010 and 2012 (Figure 4.2). The largest migration distance at the back of the stoss slope was measured up to 7.2 m between image 2 and 3 (Figure 4.2). Equating to an average migration rate of up to 4.2 m per year. This is the quickest migration measurement found in Herschel Crater thus far. This is not coherent with the data produced by Cardinale *et al.,* (2012) who measured an average dune migration rate of 0.8 m over a 3.7 earth year period

(0.2 m per earth year). This could imply that the wind velocity and threshold is somewhat higher in the centre of Herschel crater. This aligns with the dark sweeping sediment feature identified in the regional context imagery (Figure 4.1) (see chapters 4.1 and 5.1) indicting that that the strongest wind direction is southwards in central Herschel.

5.4 Superimposed Ripples

The ripples superimposed on the dune in Herschel Crater show a clear and definitive change from the 2-D straight crested ripples on the dune flanks to the complex 3-D ripples identified on the gently sloping stoss slope of the dune (Figure 4.3), similar to Hood *et al.,* (2021) study. But isn't as clearly defined where the slope gradient transitions more gently, often found at the very top (upwind) part of the stoss slope. However, where Hood *et al.,* (2021) found that the complex 3-D ripples were most common on the lower slopes of the dunes, this is not the case for Herschel dunes are the complex ripples are found over the entire stoss slopes and the sand trailing downwind from the dune (Figures 4.2 and 4.3). On the other hand, Herschel crater dunes are less affected by wind perturbations as there are no dunes directly upwind from it and the surrounding landscape north (the direction the wind is inferred to be coming from) is relatively flat. The only topographical feature in close proximity to the dune that could be affecting the airflow over the dune is the small crater northeast of it (Figure 4.1).

It is very clear from Table 4.1 that there is ripple activity in which they are migrating. The simple 2-D ripples on the flanks of the dune evidence a migratory route towards the north (Figure 4.5), indicating a northerly wind direction whereas the complex ripples on the stoss of the dune show a migration path towards the west (Figure 4.6), indicating a westerly wind direction. This contradicts the southerly wind directional airflow inferred by the barchan dune where migration and therefore sediment transport should also be towards the south. This

could be inferred as a circulatory wind movement, influenced by the surrounding topography within the crater (Cadinale *et al.,* 2012).

Table 4.3 shows the migratory length of the ripples between group 1 and group 2 (see Table 3.2) of 1.11 m. This migration rate decreases in groups 2 and 3 to 1.04 and 1.08 m. However, this then increases back to 1.11 m average migration distance in group 4. The sudden decrease in migration rates from group 1 in the 2010 period to group 2 in 2010 to 2012 could indicate a change in sediment supply or wind speed and therefore a lower wind threshold (Hood *et al.,* 2010; Cardinale *et al.,* 2012; Walker and Nickling, 2002). This could also explain the increase back to 1.11 m mean migration distance for the ripples in Group 1 (Table 3.2). The average migration rate for these ripples superimposed on the dune is 0.38 m per earth year. The average ripple migration rate for Central Herschel crater is high than that of the ripples in western Herschel crater of approximately 0.3 m per earth year (1.1 m per 3.7 year) as studied and calculated by Cardinale *et al.,* (2012). This also suggests that the wind speed and sediment transport is higher and subsequently so is the migration rates. However, in Group 3 the ripple migration rates align closest with those of Cardinale *et al.,* (2012) with a rate of 0.29 m per earth year (1.08 m over 3.7 years) indicating the wind regime on Mars is erratic.

5.5 R analysis

The impact of the GIS search distance parameter on the results of the Rubbersheet Link tool were evaluated in Table 4.1. Although the greatest distance in mean and median migration was observed between 1 m and 3 m, there was more variation using the 4 m setting. This is likely to have occurred as this search distance parameter is likely to have been overextending the search radius for matching crestline nodes. This has potentially resulted in erroneous

crestline node matches. Statistical testing also reveals that the search distance parameter has a significant ($p < 0.05$) effect on the result of migration output. This sensitivity analysis has enabled an appropriate and reliable search distance parameter to be established. This is important for the potential application of this GIS tool in helping to automate Martian crestline migration detection. However, as demonstrated, care needs to be taken when selecting search distance parameters which are likely to be site specific.

6. Conclusion

These images analysed from HiRISE (2022) evidence significant migration rates of the dune. The southwards migration of the dune is substantially faster than those that have been studied in west and eastern Herschel Crater. With a migration rate of up to 4.2 m per year compared to 0.2 m per earth year in western Herschel Crater (Cardinale *et al.,* 2012). However, while the dune migration rate presents a significant difference in migration rates, the superimposed ripples present a much slower rate of migration. The average migration rates were calculated at 0.38 m per year for the study dune which is 0.9 m more than the average ripple migration rate for western Herschel (Cardinal *et al.,* 2012). Furthermore, the migration rates for the dune appear to be more significant during the time that that ripple migration rate decreases. However, what can be concluded is that a possible explanation for why the dunes and ripples in central Herschel Crater move at a far faster rate than those of western and eastern Herschel is that its location exposes the geomorphology to more extreme wind patterns and variations in speed. Thus, affecting the sediment transport threshold rates, distance and the subsequent morphology of the dunes and ripples themselves. Additionally, the undulating features noted on the dune itself could contribute to the airflow over the dune, directly impacting the shape of the ripples superimposed. The most interesting and perhaps important finding from this study is that the ripples superimposed on this dune show a migration opposite to the inferred wind direction that the dune itself suggests (Figures 4.5 to 4.7).

The images analysed from HiRISE combined with a crest detection algorithm allowed the qualitative and quantitative assessment of dune and ripple migration in central Herschel Crater to better comprehend the wind and sediment transport complexity. Rates of migration in the ripples on the stoss slope of the dune were difficult to detect with the naked eye due

to the complexity of their formation. The 2-D ripples on the flanks of the dune showed clear migration however was not always trackable with the naked eye due to the junctions in the ripples disappearing as time moved forward. Therefore, with the rubbersheet link tool the tracking of the ripple crestlines was not only achievable but an efficient and accurate way to gain results within the short time frame of writing this paper.

6.1 Limitations

Quantification of the migration rates for the ripple crestlines used all the available data available, however this data set is small. Future studies would benefit from having a study are which has more HiRISE imagery coverage, of which the images remained the same quality. The best analysis was for the images that were merely a month apart (Image 1 and Image 2; see Table 3.1) where the ripples could be accurately tracked using their morphological patterns. To improve this, more images covering this area that are a couple of months apart rather than years, would allow for better measurements of wavelengths and migration along with a larger data set which will increase accuracy. Furthermore, the crest detection algorithm is partly automatic and partly manual relying on the user to adjust the settings to allow for the best possible outcome for data analysis.

In addition, there are still uncertainties in the physics behind the transport of sediment on Mars and how aeolian transport systems work. The grain size of these ripples is not accurately known and has been inferred from studies carried out in Gale Crater by the Curiosity Rover as well as inferences from terrestrial analogues. Future studies would further benefit from using data that has had a rover quantifying the grain sizes so that sediment transport and migration rates could be directly linked.

6.2 Future perspectives

As this dune has produced data for one of the quickest migration rates in Herschel, it would be interesting to calculate the migration rates of other central Herschel Crater dunes, specifically those that are in the most northern portion of the crater, so that they can be compared to that of this study and those that have been carried out previously to this paper.

Use of the Rubbersheet linking tool would need to be adapted for each study site, but as this was a quick and efficient way of collecting data on crestline migration rates, it would be interesting to see if this works as accurately, if not more accurately, for other sites on Mars. This would also produce lots of data quickly and therefore much more of Mars's ripples migration rates would be calculated and assessment of this would provide and interesting study for comparing those migration rates over the entirety of Mars. This could help in understanding sediment availability, wind directions and its threshold for different areas of Mars. Even more so this could potentially aid future prospective landing sites on Mars for Rovers.

References

ANDERSON, R.S. (1987). A theoretical model for aeolian impact ripples. *Sedimentology*, 34(5), pp.943–956. doi:10.1111/j.1365-3091.1987.tb00814.x.

Andreotti, B., Claudin, P., Iversen, J.J., Merrison, J.P. and Rasmussen, K.R. (2021). A lower-than-expected saltation threshold at Martian pressure and below. *Proceedings of the National Academy of Sciences*, 118(5), p.e2012386118. doi:10.1073/pnas.2012386118.

Baddock, M.C., Wiggs, G.F.S. and Livingstone, I. (2011). A field study of mean and turbulent flow characteristics upwind, over and downwind of barchan dunes. Earth Surface Processes and Landforms, 36(11), pp.1435–1448. doi:10.1002/esp.2161.

Banham, S.G., Gupta, S., Rubin, D.M., Edgett, K.S., Barnes, R., Van Beek, J., Watkins, J.A., Edgar, L.A., Fedo, C.M., Williams, R.M., Stack, K.M., Grotzinger, J.P., Lewis, K., Ewing, R.C., Day, M. and Vasavada, A.R. (2021). A Rock Record of Complex Aeolian Bedforms in a Hesperian Desert Landscape: The Stimson Formation as Exposed in the Murray Buttes, Gale Crater, Mars. *Journal of Geophysical Research: Planets,* 126(4). doi:10.1029/2020je006554.

Bourke, M.C. (2004). Aeolian sediment transport pathways and aerodynamics at troughs on Mars. *Journal of Geophysical Research*, 109(E7). doi:10.1029/2003je002155.

Bottke, W.F. and Norman, M.D. (2017). The Late Heavy Bombardment. Annual Review of Earth and Planetary Sciences, 45(1), pp.619–647. doi:10.1146/annurev-earth-063016-020131.

Bridges, N. (2010). HiRISE | *Linear Dunes and Sand Sheets in Herschel Crater* (ESP_016916_1655). [online] www.uahirise.org. Available at: https://www.uahirise.org/ESP_016916_1655.

Bridges, N.T., Ayoub, F., Avouac, J-P., Leprince, S., Lucas, A. and Mattson, S. (2012). Earth-like sand fluxes on Mars. *Nature*, 485(7398), pp.339–342. doi:10.1038/nature11022.

Bridges, N.T., Spagnuolo, M.G., de Silva, S.L., Zimbelman, J.R. and Neely, E.M. (2015). Formation of gravel-mantled megaripples on Earth and Mars: Insights from the Argentinean Puna and wind tunnel experiments. *Aeolian Research*, 17, pp.49–60. doi:10.1016/j.aeolia.2015.01.007.

Bridges, N.T., Sullivan, R., Newman, C.E., Navarro, S., van Beek, J., Ewing, R.C., Ayoub, F., Silvestro, S., Gasnault, O., Le Mouélic, S., Lapotre, M.G.A. and Rapin, W. (2017). Martian aeolian activity at the Bagnold Dunes, Gale Crater: The view from the surface and orbit. *Journal of Geophysical Research: Planets,* 122(10), pp.2077–2110. doi:10.1002/2017je005263.

Bristow, C.S. and Mountney, N.P. (2021). Aeolian Stratigraphy. *Reference Module in Earth Systems and Environmental Sciences*. doi:10.1016/b978-0-12-818234-5.00128-0.

Cabrol, N.A. and Grin, E.A. (2010). *Lakes on Mars.* Amsterdam: Elsevier.

Cantor, B.A. (2007). MOC observations of the 2001 Mars planet-encircling dust storm. *Icarus,* 186(1), pp.60–96. doi:10.1016/j.icarus.2006.08.019.

Cardinale, M., Komatsu, G., Silvestro, S. and Tirsch, D. (2012). The influence of local topography for wind direction on Mars: two examples of dune fields in crater basins. Earth Surface Processes and Landforms, 37(13), pp.1437–1443. doi:https://doi.org/10.1002/esp.3289.

Cardinale, M., Silvestro, S., Vaz, D.A., Michaels, T., Bourke, M.C., Komatsu, G. and Marinangeli, L. (2016). Present-day aeolian activity in Herschel Crater, Mars. *Icarus*, 265, pp.139–148. doi:10.1016/j.icarus.2015.10.022.

Carr, M.H. and James, W.H. (2010). Geologic history of Mars. *Earth and Planetary Science Letters*, 294(3-4), pp.185–203. doi:10.1016/j.epsl.2009.06.042.

Chapman, M.G., Neukum, G., Dumke, A., Michael, G., van Gasselt, S., Kneissl, T., Zuschneid, W., Hauber, E. and Mangold, N. (2010). Amazonian geologic history of the Echus Chasma and Kasei Valles system on Mars: New data and interpretations. *Earth and Planetary Science Letters*, 294(3-4), pp.238–255. doi:10.1016/j.epsl.2009.11.034.

Cheng, K.W., Rozel, A.B., Golabek, G.J., Ballantyne, H. and Jutzi, M. (2021). Martian Dichotomy from a Giant Impact: Mantle Convection Models. *EU General Assembly 2021*. doi:10.5194/egusphere-egu21-5745.

Chojnacki, M., Banks, M.E., Fenton, L.K. and Urso, A.C. (2019). Boundary condition controls on the high-sand-flux regions of Mars. *Geology*, 47(5), pp.427–430. doi:10.1130/G45793.1.

Daines, G. (2015). *Mariner 4 Image of Mars*. [online] NASA. Available at: https://www.nasa.gov/image-feature/mariner-4-image-of-mars [Accessed 16 Feb. 2022].

Day, M. and Zimbelman, J.R. (2021). Ripples, megaripples, and TARs, Oh, My! Recommendations regarding Mars aeolian bedform terminology. Icarus, 369, p.114647. doi:10.1016/j.icarus.2021.114647.

Dijk, T.A.G.P. v, Best, J. and Baas, A.C.W. (2021). Subaqueous and Subaerial Depositional Bedforms. *Encyclopedia of Geology*, [online] pp.771–786. Available at:

https://www.sciencedirect.com/science/article/pii/B9780081029084001879 [Accessed 19 Feb. 2022].

Diniega, S., Bramson, A.M., Buratti, B., Buhler, P., Burr, D.M., Chojnacki, M., Conway, S.J., Dundas, C.M., Hansen, C.J., McEwen, A.S., Lapôtre, M.G.A., Levy, J., Mc Keown, L., Piqueux, S., Portyankina, G., Swann, C., Titus, T.N. and Widmer, J.M. (2021). Modern Mars' geomorphological activity, driven by wind, frost, and gravity. *Geomorphology*, [online] 380, p.107627. Available at: https://www.sciencedirect.com/science/article/pii/S0169555X21000350 [Accessed 21 Jan. 2022].

Edgett, K.S. (1991). *The ejecta deposit of the ancient basin Herschel: an example of a generally unrecognized martian sedimentological unit.* [online] Available at: https://articles.adsabs.harvard.edu/pdf/1991LPSC...21..657E [Accessed 14 Feb. 2022].

Edgett, Kenneth and Malin (2000a). Examples of Martian Sandstone: Indurated, Lithified, and Cratered Eolian Dunes in MGS MOC Images.

Edgett, K.S. and Malin, M.C. (2000b). New views of Mars eolian activity, materials, and surface properties: Three vignettes from the Mars Global Surveyor Mars Orbiter Camera. Journal of Geophysical Research: Planets, 105(E1), pp.1623–1650. doi:10.1029/1999je001152.

ESRI (2023). Generate Rubbersheet Links (Editing)—ArcGIS Pro | Documentation. [online] pro.arcgis.com. Available at: https://pro.arcgis.com/en/pro-app/latest/tool-reference/editing/generate-rubbersheet-links.htm [Accessed 23 Jan. 2023].

European Space Agency (2003). Space technology goes down to Earth to support mining. [online] www.esa.int. Available at:

https://www.esa.int/About_Us/Business_with_ESA/Business_Opportunities/Space_technology_goes_down_to_Earth_to_support_mining [Accessed 21 Feb. 2023].

Favaro, E.A., Balme, M.R., Davis, J.M., Grindrod, P.M., Fawdon, P., Barrett, A.M. and Lewis, S.R. (2021). The Aeolian Environment of the Landing Site for the ExoMars Rosalind Franklin Rover in Oxia Planum, Mars. *Journal of Geophysical Research: Planets*, [online] 126(4). Available at: https://agupubs.onlinelibrary.wiley.com/doi/full/10.1029/2020JE006723 [Accessed 17 Feb. 2022].

Fenton, L.K. (2003). *Aeolian Processes on Mars: Atmospheric modeling and GIS analysis*. [Thesis] Available at: https://thesis.library.caltech.edu/877/12/fenton_phd_singleside.pdf [Accessed 25 Jan. 2022].

Gough, T.R., Hugenholtz, C.H. and Barchyn, T.E. (2021). Re-Evaluation of Large Martian Ripples in Gale Crater: Granulometric Evidence for an Impact Mechanism and Terrestrial Analogues. *Journal of Geophysical Research: Planets,* 126(12). doi:10.1029/2021je007011.

Guzewich, S.D., Lemmon, M., Smith, C.L., Martínez, G., Vicente-Retortillo, Á., Newman, C.E., Baker, M., Campbell, C., Cooper, B., Gómez-Elvira, J., Harri, A. -M., Hassler, D., Martin-Torres, F.J., McConnochie, T., Moores, J.E., Kahanpää, H., Khayat, A., Richardson, M.I., Smith, M.D. and Sullivan, R. (2019). Mars Science Laboratory Observations of the 2018/Mars Year 34 Global Dust Storm. *Geophysical Research Letters*, [online] 46(1), pp.71–79. Available at: https://agupubs.onlinelibrary.wiley.com/doi/full/10.1029/2018GL080839 [Accessed 16 Feb. 2022].

Hartmann, W.K. and Werner, S.C. (2010). Martian Cratering 10. Progress in use of crater counts to interpret geological processes: Examples from two debris aprons. *Earth and*

Planetary Science Letters, [online] 294(3-4), pp.230–237. Available at: https://www.sciencedirect.com/science/article/abs/pii/S0012821X09005901 [Accessed 18 Feb. 2022].

Hayward, R.K., Fenton, L.K. and Titus, T.N. (2014). Mars Global Digital Dune Database (MGD3): Global dune distribution and wind pattern observations. *Icarus*, [online] 230, pp.38–46. Available at: https://www.sciencedirect.com/science/article/pii/S0019103513001711 [Accessed 15 Feb. 2022].

Heap, M.J., Byrne, P.K. and Mikhail, S. (2017). Low surface gravitational acceleration of Mars results in a thick and weak lithosphere: Implications for topography, volcanism, and hydrology. Icarus, 281, pp.103–114. doi:10.1016/j.icarus.2016.09.003.

Hersen, P. and Douady, S. (2005). Collision of barchan dunes as a mechanism of size regulation. Geophysical Research Letters, 32(21). doi:https://doi.org/10.1029/2005gl024179.

HiRISE University of Arizona (2022). HiRISE | *High Resolution Imaging Science Experiment*. [online] www.uahirise.org. Available at: https://www.uahirise.org/ [Accessed 28 Oct. 2021].

Hood, D.R., Ewing, R.C., Roback, K.P., Runyon, K., Avouac, J.-P. . and McEnroe, M. (2021). Inferring Airflow Across Martian Dunes From Ripple Patterns and Dynamics. *Frontiers in Earth Science*, 9. doi:10.3389/feart.2021.702828.

Hughes, M., Harris, P.T., Brooke, B. and Geoscience Australia (2010). Seabed exposure and ecological disturbance on Australia's continental shelf : potential surrogates for marine biodiversity. Canberra: Geoscience Australia.

Irwin, R.P. and Howard, A.D. (2002). Drainage basin evolution in Noachian Terra Cimmeria, Mars. *Journal of Geophysical Research*, [online] 107(E7). Available at:

https://citeseerx.ist.psu.edu/viewdoc/download?doi=10.1.1.596.2545&rep=rep1&type=pdf [Accessed 17 Feb. 2022].

JPL NASA (2020). *Curiosity Spots a Dust Devil in the Hills*. [online] NASA Jet Propulsion Laboratory (JPL). Available at: https://www.jpl.nasa.gov/images/pia24039-curiosity-spots-a-dust-devil-in-the-hills [Accessed 18 Feb. 2022].

Kass, D.M., Schofield, J.T., Kleinböhl, A., McCleese, D.J., Heavens, N.G., Shirley, J.H. and Steele, L.J. (2020). Mars Climate Sounder Observation of Mars' 2018 Global Dust Storm. *Geophysical Research Letters*, [online] 47(23). Available at: https://agupubs.onlinelibrary.wiley.com/doi/full/10.1029/2019GL083931 [Accessed 16 Feb. 2022].

Lapôtre, M.G.A., Ewing, R.C. and Lamb, M.P. (2021). An Evolving Understanding of Enigmatic Large Ripples on Mars. *Journal of Geophysical Research: Planets*, [online] 126(2). Available at: https://agupubs.onlinelibrary.wiley.com/doi/full/10.1029/2020JE006729 [Accessed 16 Feb. 2022].

Lapotre, M.G.A., Ewing, R.C., Weitz, C.M., Lewis, K.W., Lamb, M.P., Ehlmann, B.L. and Rubin, D.M. (2018). Morphologic Diversity of Martian Ripples: Implications for Large-Ripple Formation. *Geophysical Research Letters*, [online] 45(19), pp.10, 229–10, 239. Available at: https://agupubs.onlinelibrary.wiley.com/doi/pdfdirect/10.1029/2018GL079029 [Accessed 19 Feb. 2022].

Lü, P., Dong, Z. and Rozier, O. (2018). The Combined Effect of Sediment Availability and Wind Regime on the Morphology of Aeolian Sand Dunes. *Journal of Geophysical Research: Earth Surface*, [online] 123(11), pp.2878–2886. Available at:

https://agupubs.onlinelibrary.wiley.com/doi/full/10.1029/2017JF004361 [Accessed 18 Feb. 2022].

mars.nasa.gov (2022). *NASA's InSight Sees Power Levels Stabilize After Dust Storm*. [online] NASA's Mars Exploration Program. Available at: https://mars.nasa.gov/news/9110/nasas-insight-sees-power-levels-stabilize-after-dust-storm/ [Accessed 16 Feb. 2022].

mars.nasa.gov (n.d.). *THE 1600s (The first telescopes see Mars)*. [online] Nasa.gov. Available at: https://mars.nasa.gov/allaboutmars/mystique/history/1600/ [Accessed 14 Feb. 2022].

McKee (1979). A study of global sand seas. Professional Paper. doi:https://doi.org/10.3133/pp1052.

Nummi, E. (2016). Technology from Space May Help Mining on Earth. [online] Advancing Mining. Available at: https://www.thermofisher.com/blog/mining/technology-from-space-may-help-mining-on-earth/ [Accessed 21 Feb. 2023].

NASA (2000). *Mars Exploration Past Missions*. [online] NASA. Available at: https://www.nasa.gov/mission_pages/mars/missions/index-past.html [Accessed 14 Feb. 2022].

Neukum, G., Basilevsky, A.T., Kneissl, T., Chapman, M.G., van Gasselt, S., Michael, G., Jaumann, R., Hoffmann, H. and Lanz, J.K. (2010). The geologic evolution of Mars: Episodicity of resurfacing events and ages from cratering analysis of image data and correlation with radiometric ages of Martian meteorites. *Earth and Planetary Science Letters*, [online] 294(3-4), pp.204–222. Available at: https://www.sciencedirect.com/science/article/abs/pii/S0012821X09005305 [Accessed 18 Feb. 2022].

Outen, E. (2009). *NASA - Exploration: Then and Now*. [online] www.nasa.gov. Available at: https://www.nasa.gov/audience/foreducators/exploration-then-and-now.html [Accessed 14 Feb. 2022].

Rabkin, E.S. (2005). *Mars : a tour of the human imagination*. Westport, Conn.: Praeger Publishers.

Renno, N.O., Wong, A.-S. and Atreya, S.K. (2003). Electrical discharges and broadband radio emission by Martian dust devils and dust storms. *Geophysical Research Letters*, [online] 30(22). Available at: https://agupubs.onlinelibrary.wiley.com/doi/pdf/10.1029/2003GL017879 [Accessed 31 Jan. 2022].

Runyon, K.D., Bridges, N.T., Ayoub, F., Newman, C.E. and Quade, J.J. (2017). An integrated model for dune morphology and sand fluxes on Mars. *Earth and Planetary Science Letters*, 457, pp.204–212. doi:10.1016/j.epsl.2016.09.054.

Salvatore, M.R. and Levy, J.S. (2021). The McMurdo Dry Valleys of Antarctica: a geological, environmental, and ecological analog to the Martian surface and near surface. *Mars Geological Enigmas*, [online] pp.291–332. Available at: https://www.sciencedirect.com/science/article/pii/B9780128202456000112 [Accessed 31 Jan. 2022].

Silvestro, S., Chojnacki, M., Vaz, D.A., Cardinale, M., Yizhaq, H. and Esposito, F. (2020). Megaripple Migration on Mars. *Journal of Geophysical Research: Planets*, [online] 125(8). Available at: https://agupubs.onlinelibrary.wiley.com/doi/full/10.1029/2020JE006446 [Accessed 17 Feb. 2022].

Silvestro, S., Di Achille, G. and Ori, G.G. (2010). Dune morphology, sand transport pathways and possible source areas in east Thaumasia Region (Mars). *Geomorphology*, [online] 121(1-2), pp.84–97. Available at: https://www.sciencedirect.com/science/article/pii/S0169555X09003377 [Accessed 16 Feb. 2022].

Silvestro, S., Fenton, L.K. and Vaz, D.A., 2010, March. Ripple migration and small modifications of active dark dunes in Nili Patera (Mars). In *41st Annual Lunar and Planetary Science Conference* (No. 1533, p. 1820).

Silvestro, S., Fenton, L.K., Vaz, D.A., Bridges, N.T. and Ori, G.G. (2010). Ripple migration and dune activity on Mars: Evidence for dynamic wind processes. *Geophysical Research Letters*, [online] 37(20). Available at: https://agupubs.onlinelibrary.wiley.com/doi/full/10.1029/2010GL044743 [Accessed 16 Feb. 2022].

Silvestro, S., Vaz, D.A., Fenton, L.K. and Geissler, P.E. (2011). Active aeolian processes on Mars: A regional study in Arabia and Meridiani Terrae. *Geophysical Research Letters*, [online] 38(20). Available at: https://agupubs.onlinelibrary.wiley.com/doi/full/10.1029/2011GL048955 [Accessed 18 Feb. 2022].

Silvestro, S., Vaz, D.A., Yizhaq, H. and Esposito, F. (2016). Dune-like dynamic of Martian Aeolian large ripples. *Geophysical Research Letters*, 43(16), pp.8384–8389. doi:10.1002/2016gl070014.

Smith, M.D. (2019). THEMIS Observations of the 2018 Mars Global Dust Storm. *Journal of Geophysical Research: Planets*, [online] 124(11), pp.2929–2944. Available at:

https://agupubs.onlinelibrary.wiley.com/doi/full/10.1029/2019JE006107 [Accessed 16 Feb. 2022].

Smrekar, S.E. (2004). Geologic evolution of the Martian dichotomy in the Ismenius area of Mars and implications for plains magnetization. *Journal of Geophysical Research*, [online] 109(E11). Available at: https://agupubs.onlinelibrary.wiley.com/doi/full/10.1029/2004JE002260 [Accessed 18 Feb. 2022].

Sostre-Cortes, J. and Diniega, S. (2021). Quest for Present-day Dune Evolution on Mars. *NASA ADS*, [online] 53, p.213.03. Available at: https://ui.adsabs.harvard.edu/abs/2021DPS....5321303S/abstract [Accessed 17 Feb. 2022].

Sullivan, R., Arvidson, R., Bell, J.F., Gellert, R., Golombek, M., Greeley, R., Herkenhoff, K., Johnson, J., Thompson, S., Whelley, P. and Wray, J. (2008). Wind-driven particle mobility on Mars: Insights from Mars Exploration Rover observations at 'El Dorado' and surroundings at Gusev Crater. *Journal of Geophysical Research*, 113(E6). doi:10.1029/2008je003101.

Sullivan, R., Kok, J.F., Katra, I. and Yizhaq, H. (2020). A Broad Continuum of Aeolian Impact Ripple Morphologies on Mars is Enabled by Low Wind Dynamic Pressures. *Journal of Geophysical Research: Planets*, [online] 125(10). Available at: https://agupubs.onlinelibrary.wiley.com/doi/10.1029/2020JE006485 [Accessed 16 Feb. 2022].

Tanaka, K.L. and Hartmann, W.K. (2012). The Planetary Time Scale. *The Geologic Time Scale*, [online] pp.275–298. Available at: file:///C:/Users/evisick/Downloads/article.pdf [Accessed 17 Feb. 2022].

Telfer, M.W., Fyfe, R.M. and Lewin, S. (2015). Automated mapping of linear dunefield morphometric parameters from remotely-sensed data. *Aeolian Research*, 19, pp.215–224. doi:10.1016/j.aeolia.2015.03.001.

The Planetary Society (2022). *Topographic map of Mars*. [online] The Planetary Society. Available at: https://www.planetary.org/space-images/topographic-map-of-mars [Accessed 18 Feb. 2022].

Tsoar H. (2001) Types of Aeolian Sand Dunes and Their Formation. In: Balmforth N.J., Provenzale A. (eds) Geomorphological Fluid Mechanics. Lecture Notes in Physics, vol 582. Springer, Berlin, Heidelberg. https://doi.org/10.1007/3-540-45670-8_17

Vaucher, R. and Dashtgard, S.E. (2021). Nearshore Bedforms. *Reference Module in Earth Systems and Environmental Sciences*. [online] Available at: https://www.sciencedirect.com/science/article/pii/B9780128182345000936 [Accessed 19 Feb. 2022].

Venditti, J.G. (2005). Bed form initiation from a flat sand bed. *Journal of Geophysical Research*, [online] 110(F1). Available at: https://agupubs.onlinelibrary.wiley.com/doi/full/10.1029/2004JF000149 [Accessed 19 Feb. 2022].

Walker, I.J. and Nickling, W.G. (2002). Dynamics of secondary airflow and sediment transport over and in the lee of transverse dunes. Progress in Physical Geography: Earth and Environment, 26(1), pp.47–75. doi:https://doi.org/10.1191/0309133302pp325ra.

Wang, P., Zhang, J. and Huang, N. (2019). A theoretical model for aeolian polydisperse-sand ripples. *Geomorphology*, 335, pp.28–36. doi:10.1016/j.geomorph.2019.03.013.

Yizhaq, H. and Katra, I. (2015). Longevity of aeolian megaripples. *Earth and Planetary Science Letters*, 422, pp.28–32. doi:10.1016/j.epsl.2015.04.004.

Yizhaq, H., Swet, N., Saban, L. and Katra, I. (2020). Rediscovery of the Fluid Drag Ripples in Wind Tunnel Experiments. *Sixth International Planetary Dune Workshop 2188*.

Zheng, Z., Du, S., Taubenböck, H. and Zhang, X. (2022). Remote sensing techniques in the investigation of aeolian sand dunes: A review of recent advances. *Remote Sensing of Environment*, [online] 271, p.112913. Available at: https://www.sciencedirect.com/science/article/pii/S003442572200027X [Accessed 17 Feb. 2022].

Zimbelman, J.R., Williams, S.H. and Johnston, A.K. (2012). Cross-sectional profiles of sand ripples, megaripples, and dunes: a method for discriminating between formational mechanisms. *Earth Surface Processes and Landforms,* 37(10), pp.1120–1125. doi:10.1002/esp.3243.

Appendix A: R Script

```
library(tidyverse)

##Mars crest data analysis##

Crestlines = read.csv(file.choose()) #to load in gis data

head(Crestlines)

#This is the descriptive stats for crest migration by year
according to the rubbersheeting method

Crestlines %>%

  group_by(Group) %>%

  dplyr::summarize(Mean = mean(SHAPE_Length, na.rm=TRUE),

                   Median = median(SHAPE_Length, na.rm=TRUE),

                   SD  =  sd(SHAPE_Length,  na.rm=TRUE),CV  =
(SD/Mean),

                   PercentageCV = (SD/Mean*100))

#Sensitivity analysis

SD_1m = read.csv(file.choose()) #to load in gis data, search
dist. 1m

SD_3m = read.csv(file.choose()) #to load in gis data, search
dist. 3m

SD_4m = read.csv(file.choose()) #to load in gis data, search
dist. 4m
```

```
head(SD_1m) #preview data

Sample1m=SD_1m[sample(1:nrow(SD_1m),4000), ]

shapiro.test(Sample1m$SHAPE_Length)    #NORMALITY    TEST    FOR
MIGRATION DISTANCE

#if  the  p-value  is  less  than  0.05  then  data  not  normally
distributed

#Plot to visualise data distrubtion QQ plot

qqnorm(SD_1m$SHAPE_Length, pch = 1, frame = FALSE)

qqline(SD_1m$SHAPE_Length, col = "steelblue", lwd = 2)

#selecting  a  statistical  test  for  difference:  wilcox  as  not
normally distributed

#1m vs 3m

wilcox.test(x = SD_1m$SHAPE_Length, y = SD_3m$SHAPE_Length)

#3m vs 4m

wilcox.test(x = SD_3m$SHAPE_Length, y = SD_4m$SHAPE_Length)

SD_1m %>%

  dplyr::summarize(Mean = mean(SHAPE_Length, na.rm=TRUE),

                   Median = median(SHAPE_Length, na.rm=TRUE),

                   SD   =   sd(SHAPE_Length,   na.rm=TRUE),CV   =
(SD/Mean),

                   PercentageCV = (SD/Mean*100))
```

```
SD_3m %>%
  dplyr::summarize(Mean = mean(SHAPE_Length, na.rm=TRUE),
                   Median = median(SHAPE_Length, na.rm=TRUE),
                   SD   =   sd(SHAPE_Length,   na.rm=TRUE),CV   =
(SD/Mean),
                   PercentageCV = (SD/Mean*100))
SD_4m %>%
  dplyr::summarize(Mean = mean(SHAPE_Length, na.rm=TRUE),
                   Median = median(SHAPE_Length, na.rm=TRUE),
                   SD   =   sd(SHAPE_Length,   na.rm=TRUE),CV   =
(SD/Mean),
                   PercentageCV = (SD/Mean*100))
#BOX PLOTS
par(mfrow=c(1,1))
boxplot(SD_1m$SHAPE_Length, SD_3m$SHAPE_Length,
        ylab = "Crestline Migration Distance (metres)",
        xlab = "QGIS Parameter Search Distance",
        names = c("1 m setting", "3 m setting"))
#BOX PLOTS 1,3 and 4 m
par(mfrow=c(1,1))
```

```
boxplot(SD_1m$SHAPE_Length,                SD_3m$SHAPE_Length,
SD_4m$SHAPE_Length,
        ylab = "Crestline Migration Distance (metres)",
        xlab = "QGIS Parameter Search Distance",
        names = c("1 m setting", "3 m setting", "4 m setting"))
```